Atmos. Meas. Tech. Discuss., 8, 6993–7056, 2015
www.atmos-meas-tech-discuss.net/8/6993/2015/
doi:10.5194/amtd-8-6993-2015

Atmospheric Measurement Techniques Discussions
Open Access

Overview of the O3M SAF GOME-2 operational atmospheric composition and UV radiation data products and data availability

S. Hassinen[1], D. Balis[2], H. Bauer[3], M. Begoin[3], A. Delcloo[4], K. Eleftheratos[5], S. Gimeno Garcia[3], J. Granville[6], M. Grossi[3], N. Hao[3], P. Hedelt[3], F. Hendrick[6], M. Hess[7], K.-P. Heue[3], J. Hovila[1], H. Jønch-Sørensen[8], N. Kalakoski[1], S. Kiemle[3], L. Kins[7], M. E. Koukouli[2], J. Kujanpää[1], J.-C. Lambert[6], C. Lerot[6], D. Loyola[3], A. Määttä[1], M. Pedergnana[3], G. Pinardi[6], F. Romahn[3], M. van Roozendael[6], R. Lutz[3], I. De Smedt[6], P. Stammes[9], W. Steinbrecht[7], J. Tamminen[1], N. Theys[6], L. G. Tilstra[9], O. N. E. Tuinder[9], P. Valks[3], C. Zerefos[5], W. Zimmer[3], and I. Zyrichidou[2]

[1]Finnish Meteorological Institute, Helsinki, Finland
[2]Aristotle University of Thessaloniki, Thessaloniki, Greece
[3]Deutsches Zentrum für Luft- und Raumfahrt, DLR, Oberpfaffenhofen, Germany
[4]Royal Meteorological Institute, Brüssel, Belgium
[5]Mariolopoulos – Kanaginis Foundation, Athens, Greece

[6]Belgian Institute for Space Aeronomy, BIRA-IASB, Brussels, Belgium
[7]German Weather Service, Offenbach, Germany
[8]Danish Meteorological Institute, Copenhagen, Danmark
[9]Royal Netherlands Meteorological Institute, De Bilt, the Netherlands

Received: 29 April 2015 – Accepted: 10 June 2015 – Published: 09 July 2015

Correspondence to: S. Hassinen (seppo.hassinen@fmi.fi)

Published by Copernicus Publications on behalf of the European Geosciences Union.

AMTD
8, 6993–7056, 2015

Abstract

The three GOME-2 instruments will provide unique and long data sets for atmospheric research and applications. The complete time period will be 2007–2022, including the period of ozone depletion as well as the beginning of ozone layer recovery. Besides ozone chemistry, the GOME-2 products are important e.g. for air quality studies, climate modeling, policy monitoring and hazard warnings. The heritage for GOME-2 is in the ERS/GOME and Envisat/SCIAMACHY instruments. The current Level 2 (L2) data cover a wide range of products such as trace gas columns (NO_2, BrO, H_2CO, H_2O, SO_2), tropospheric columns of NO_2, total ozone columns and vertical ozone profiles in high and low spatial resolution, absorbing aerosol indices from the main science channels as well as from the polarization channels (AAI, AAI-PMD), Lambertian-equivalent reflectivity database, clear-sky and cloud-corrected UV indices and surface UV fields with different weightings and photolysis rates. The Ozone Monitoring and Atmospheric Composition Satellite Application Facility (O3M SAF) processing and data dissemination is operational and running 24/7. Data quality is quarantined by the detailed review processes for the algorithms, validation of the products as well as by a continuous quality monitoring of the products and processing. This is an overview paper providing the O3M SAF project background, current status and future plans to utilization of the GOME-2 data. An important focus is the provision of summaries of the GOME-2 products including product principles and validation examples together with the product sample images. Furthermore, this paper collects the references to the detailed product algorithm and validation papers.

1 Introduction

The anthropogenic changes in atmospheric composition and chemistry cause climate warming, pollution and changes in the oxidizing efficiency of atmosphere. All these have a major impact on the living conditions on the Earth. Understanding the evolution

AMTD
8, 6993–7056, 2015

of the atmospheric composition as well as the coupling between climate and chemistry is a challenge which requires an efficient global monitoring system of ozone and other trace gases, ultraviolet radiation, primary pollutants and pre-cursors, together with the distribution and properties of aerosols. With the recent volcanic eruptions posing hazards and economic losses to the European aviation business, detection of volcanic sulfur dioxide and aerosols from satellites has become an important part of the remote sensing of the atmosphere. Satellite-based observations form an important part of this global observing system as they can provide global, three-dimensional coverage with a regular repeat cycle.

The Global Ozone Monitoring Experiment-2 (GOME-2) instrument is targeted to fulfill these expectations. It is one of the new-generation European instruments carried on Metop platforms which are part of the EUMETSAT Polar System (EPS). The GOME-2 instruments will continue the long-term monitoring of atmospheric constituents started by GOME on ERS-2 (Callies et al., 2000; Munro et al., 2006) and SCIAMACHY on Envisat (Bovensmann et al., 1999). As an operational mission, continuity of observations is ensured by three identical instruments onboard three Metop platforms: A, B and C: the first was launched in 2006, the second in 2012 and the last one will be launched in 2017. The GOME-2 instruments will provide unique long term data sets of 15 years related to atmospheric composition and surface ultra violet (UV) radiation using stable retrieval techniques. The GOME-2 is set to make a significant contribution towards climate and atmospheric research, whilst providing near real-time data for use in air quality forecasting.

The provision of an operational 24/7 service is also an important response to the expectations outlined above. Thus, the Level 2 (L2) GOME-2 product development, processing, dissemination and user services are the responsibility of the Satellite Application Facility on Ozone and Atmospheric Chemistry Monitoring (O3M SAF) project which is an integral part of the distributed EUMETSAT Application Ground Segment. The product development includes extensive product review steps focusing on product requirements, product algorithms as well as validation results. Furthermore, the

AMTD
8, 6993–7056, 2015

ground segment processing chains have been reviewed keeping in mind the 24/7 requirement for processing and dissemination. The production includes continuous quality control for the processing and products. These requirements for production fulfills the expectations of the key users, like CAMS (Copernicus Atmosphere Monitoring Service), ECMWF (The European Centre for Medium-Range Weather Forecasts) and VAACs (Volcanic Ash Advisory Centres). The other areas where the GOME-2 products are used, cover a wide range of applications from monitoring of volcanic emissions to atmospheric research and from the air quality assessments to UV radiation warnings. Other users of the GOME-2 data include SACS (Support to Aviation Control Service), WMO (World Meteorological Organization) programs and research institutes and health organizations. GOME-2 products from the O3M SAF project are the only European operational products of this class with a long period of data availability and quality control.

The current L2 data cover a wide range of products, such as ozone and trace gas columns (total and tropospheric NO_2, total BrO, HCHO, H_2O, SO_2), vertical ozone profiles in high and low spatial resolution, absorbing aerosol indices from the main science channels as well as from the polarization channels (AAI, AAI-PMD), Lambertian-equivalent reflectivity database, clear-sky and cloud-corrected UV indices and surface UV fields with different weightings and NO_2 and O_3 photolysis rates. In future, the products will include tropospheric columns of O_3 and BrO as well as special climatic data sets of H_2O and NO_2. The products are disseminated in the Near Real Time (NRT) streams via EUMETCast, which is a multi-service dissemination system based on standard Digital Video Broadcast (DVB) technology and uses commercial telecommunication geostationary satellites to multi-cast files (data and products) to a wide user community. Furthermore, the NRT products are available via WMO GTS (Global Telecommunication System) whereas data-records and offline products are available via the O3M SAF data services and EUMETSAT Data Center.

The O3M SAF started in 2004 with a development phase and the first operational Continuous Development and Operations Phase (CDOP) started in 2007. The Phase

AMTD
8, 6993–7056, 2015

2 (CDOP-2) started in 2012 and the third will start in 2017. Besides GOME-2 products, the project, together with the EUMETSAT Central Facilities, will also provide also some new IASI products developed by LATMOS (Laboratoire Atmosphères, Milieux, Observations Spatiales) and ULB (Université libre de Bruxelles). The first IASI product, carbon monoxide, will be released in fall 2015. The project description as well as product information, documentation, Helpdesk, user services and the dissemination services are available from the project web site (http://o3msaf.fmi.fi).

The purpose of this paper is to give an overall description of the GOME-2 activities and products provided by the O3M SAF project. The paper is organized as follows: the instrument and ground segment, retrieved parameters with key validation summary, emerging products and dissemination and user services.

2 The GOME-2 instrument

The GOME-2 (The Global Ozone Monitoring Experiment-2) instruments onboard the Metop satellite platforms are direct successors to GOME instrument that was flying onboard the ERS-2 platforms and thus, the basic concept is the same. However, quite a number of changes to the GOME instrument design have been imposed by the fact that Metop is a very different satellite from ERS-2, designed for a different orbit. For example, the new orbit imposes a different viewing angle to the Sun, for in-orbit calibration purposes, and some moderate changes in the instrument's thermal environment (Callies et al., 2000). The scientific objectives have a direct heritage from the GOME mission. The GOME general objectives, as listed in Burrows et al. (1993), were: (a) to improve understanding of the processes controlling global bio-geochemical cycles in the troposphere and stratosphere and (b) to monitor natural and anthropogenic changes in the composition of the atmosphere. The more detailed scientific objectives for GOME and thus also for GOME-2 and based on Burrows et al. (1993) are: measurement of total column and stratospheric and tropospheric profiles of ozone, measurements of other trace gases involved in ozone photochemistry (e.g. NO_2, OClO,

AMTD
8, 6993–7056, 2015

BrO), measurement of column amounts of H_2O, measurements of pollutants such as SO_2 and H_2CO and measurements of atmospheric aerosols and spectral reflectance. The GOME-2 instrument was designed and build at the time of the strongest ozone depletion and thus, one of it's main objectives is to monitor ozone, ozone chemistry and the development of the ozone depletion. The ozone layer is on track to recovery, states the WMO Assessment for Decision-Makers: Scientific Assessment of Ozone Depletion: 2014 (World Meteorological Organization 2014). Thus, the scientific value of the GOME-2 instrument measurements will also continue in the future.

The GOME-2 instrument is a nadir looking scanning UV-VIS spectrometer that measures backscattered solar light. GOME-2 comprises four main optical channels of 1024 pixels giving in total 4096 spectral channels for a range of 240–790 nm and a spectral resolution of 0.26–0.51 nm. Furthermore, the two Polarization Measurement Devices (PMDs) containing the same type of arrays for measurement of linearly polarized intensity in two perpendicular directions provide 30 broad-band polarization channels.

The Metop satellites are flying on a sun-synchronous orbit with an equator crossing time of about 09:30 LT (descending node) and a repeat cycle of 29 days. The default swath width of the GOME-2 scan is 1920 km, which gives a nadir pixel size of 80 km × 40 km (across-track × along-track) and enables global coverage in about 1.5 days. The current primary GOME-2 onboard Metop-B platform (GOME-2B) is operated in this mode whereas the older, GOME-2 onboard Metop-A platform (GOME-2A) is operated in a reduced swath width mode with a swath width of 960 km and nadir ground pixel size of 40 km × 40 km. The GOME-2A is expected to be operational until the launch of the Metop-C platform in 2017.

More details with the GOME-2 fact-sheet may be found from http://www.eumetsat.int/website/home/Satellites/CurrentSatellites/Metop/MetopDesign/GOME2/index.html.

AMTD
8, 6993–7056, 2015

3 L0 and L1 processing

The EUMETSAT central processing facility, located in Darmstadt, is responsible for the processing of all GOME-2 data up to Level 1b. This processing is carried out within the Core Ground Segment (CGS) by the GOME-2 Product Processing Facility (PPF) which converts raw instrument data (Level 0 data stream) into time-stamped, geolocated, and fully spectrally and radiometrically calibrated radiances or irradiances (Level 1b data stream). The Level 1b data is delivered to the L2 processing centers in Near Real Time via EUMETCast. The details of GOME-2 instrument design, calibration and L1 processing will be available from Munro et al. (2015).

4 L2 processing and archiving services

The O3M SAF GOME-2 L2 products are developed and processed in a distributed EUMETSAT ground segment with four processing centers and two archives (Fig. 1). The Leading Entity, FMI (Finnish Meteorological Institute), processes and archives the offline UV products as well as archives the offline absorbing aerosol index and vertical ozone profile products and LER (Lambertian equivalent reflectivity) data set processed at KNMI (Royal Netherlands Meteorological Institute). DLR (Deutsches Zentrum für Luft- und Raumfahrt) processes, archives and disseminates total and tropospheric trace gas column products. The NRT products are disseminated via EUMETCast and WMO GTS network directly by the processing centers except the NRT UV products which are processed in by the Danish Meteorological Institute (DMI) and distributed via http and FTP. The internal O3M SAF product, assimilated GOME-2 total ozone analysis and forecast (Eskes et al., 2003), is based on O3M SAF GOME-2 total ozone and processed by KNMI and used by DMI in NRT UV production Furthermore, the internal cloud products needed for trace gas retrievals are processed by DLR.

The O3M SAF GOME-2 products undergo an extensive review process during the development process before they can be declared operational. The validation activities

AMTD
8, 6993–7056, 2015

are an important part of this review process. The validation is mainly performed by the specialized validation entities AUTH (Aristotle University of Thessaloniki), BIRA (Belgian Institute for Space Aeronomy), DWD (German Weather Service) and RMI (Royal Meteorological Institute). On top of that, online quality monitoring services have been implemented by the processing and validation institutes so that the product users may check the latest information regarding the product quality. Online quality monitoring uses external satellite and ground-based data and plotting of trends and special parameters. The data delay is from a few minutes up to a few days depending on what kind of method is used. Furthermore, special user services of climatological proxies and BEAT (Basic Envisat Atmospheric Toolbox) support are provided by MKF (Mariolopoulos – Kanaginis Foundation) and the S & T private company respectively.

All the product documentation, such as ATBDs (Algorithm Theoretical Basis Documents), validation reports and Product User Manuals (PUMs) as well as ordering interfaces and links to validation and online quality monitoring sites are available from the project web site: http://o3msaf.fmi.fi.

5 Operational O3M SAF GOME-2 products

The currently operational and available products are shown in Table 1. The following sub-chapters provide an overview of those products with some validation examples. Most of the products are available both from the Metop-A instrument as well as from the Metop-B instrument. By using both of those instruments together, global coverage may be obtained in one day. Merged L3 products will be available during the CDOP-3 phase, starting in 2017.

5.1 Vertical column densities of ozone and other trace gases

The vertical column densities of ozone and other trace gases are retrieved with the GDP (GOME Data Processor). The retrieval of the trace gas column products with the

AMTD
8, 6993–7056, 2015

GDP is based on the Differential Optical Absorption Spectroscopy (DOAS) method Platt and Stutz (2008).The latest operational version is 4.7 whereas the updated version 4.8 will be implemented in fall 2015. Table 2 lists the GOME-2 trace gas column and cloud products generated by the O3MSAF, with the corresponding wavelength regions used for the retrieval.

5.1.1 Total ozone column

Total ozone columns are retrieved from GOME-2 (ir)radiance spectra using the DOAS method (Platt and Stutz, 2008) in the wavelength region 325–335 nm (Huggins absorption band). The fitting includes an effective temperature for the ozone absorption, an NO_2 absorption cross-section, and scaling factors for interference due to the Ring effect. The retrieved ozone slant column densities are converted to vertical columns (VCD) using an iterative air mass factor (AMF). A detailed description of the GOME-2 total ozone column algorithm can be found in Van Roozendael et al. (2006); Loyola et al. (2011) and Hao et al. (2014). Figure 2 shows one example of the total ozone product: the Antarctic ozone hole for 2 October 2014 measured from GOME-2A and GOME-2B when the minimum total ozone column reached around 120 DU.

The total ozone NRT and offline products from GOME-2A and GOME-2B are periodically validated and routinely monitored for their quality. For this purpose, in the frame of the EUMETSAT O3M SAF project, a dedicated web-portal is available at http://lap3.physics.auth.gr/eumetsat. In this portal, online comparisons with quality assured ground-based total ozone measurements are available. The reference data for the offline total ozone comparisons are archived Brewer, Dobson and M-124 total ozone data, as these are deposited at the World Ozone and UV Data Centre (http://www.woudc.org) and are employed after being thoroughly controlled for their quality. These online comparisons are routinely and automatically updated every month. For the near real-time total ozone comparisons, near-real time Brewer and Dobson total ozone data, deposited in the World Meteorological Organisation Ozone Mapping

AMTD
8, 6993–7056, 2015

Center (http://lap.physics.auth.gr/ozonemaps2/), are downloaded and compared to the GOME-2A and GOME-2B near real-time observations on a weekly basis.

Comparison results for the GOME-2A offline data for the period 2007–2011, processed with GDP4.4 (Loyola et al., 2011), have been previously presented by Koukouli et al. (2012) indicating that GOME-2 total ozone data agree at the 1 % level with the ground-based measurements as well as other satellite instrument datasets, showing a small dependency on solar zenith angle for angles less than 75° and almost no dependency on cloud fraction and cloud top pressure. Results from an initial validation of the GOME-2B offline data, processed with GDP4.7 for the year 2013, have been presented in Hao et al. (2014). These results show an excellent consistency with coincident GOME-2A total ozone measurements. In Fig. 3 we present an updated time series of the differences between GOME-2A and GOME-2B vs. Dobson and Brewer total ozone data, averaged over the Northern Hemisphere for the period 2007–2014 inclusive. This confirms the consistency between the two satellite data sets as well as their long-term stability. The use of BDM (Brion, Daumont, and Malicet) absorption cross sections (Malicet et al., 1995) in the GDP4.7 version of the algorithm explains the overestimation of GOME-2 data, compared with the results presented earlier by Koukouli et al. (2012). Both satellites are consistent over the Northern Hemisphere with negligible latitudinal dependence, while over the Southern Hemisphere there is a systematic difference of 1 % between the two satellite instruments.

In addition to the comparisons with the ground-based data, GOME-2 total ozone has been analyzed against dynamical proxies such as the QBO, ENSO, NAO, etc. The target is to verify the amplitude of these proxies in the GOME-2 total ozone and if these proxies are consistent with other satellite date sets, as well as model simulations (Eleftheratos et al., 2015). The upper panel of Fig. 4 shows the amplitude of ENSO in the tropics as estimated from analyzing GOME-2, SBUV v8.6 (McPeters et al., 2013) and the merged GOME/SCIAMACHY/GOME2 CCI (Lerot et al., 2014) data sets together with the Southern Oscillation Index (SOI). The statistical analysis performed indicates consistent estimates of the ENSO signal from all three data sets, showing an amplitude

AMTD
8, 6993–7056, 2015

of 12 DU which corresponds to 4 % of the annual mean. The lower panel presents the corresponding analysis for the North Atlantic Oscillation for the northern mid-latitude region. Also here the NAO signal is consistent between the three datasets, showing an amplitude of 18 DU which corresponds to 6 % of the annual mean.

A wide community is using the GOME-2 total ozone product provided by the O3M SAF. Since October 2013, total ozone column data are assimilated in the GMES/Copernicus (Global Monitoring for Environment and Security) atmosphere core service project MACC-II (Monitoring Atmospheric Composition and Climate – Interim Implementation) NRT system. The GOME-2 ozone columns are also used in the Integrated Forecast System (IFS) of the European Centre for Medium-Range Weather Forecasts (ECMWF). Furthermore, the GOME-2 total ozone data was used in the WMO/UNEP Scientific Assessment of Ozone Depletion reports of 2010 (World Meteorological Organization 2011) and 2014 (in preparation). Other users are WMO WOUDC (World Ozone and Ultraviolet Radiation Data Centre), WMO OMP (Ozone Mapping Centre), DLR WDC-RSAT (World Data Center for Remote Sensing of the Atmosphere), and ESA TEMIS (Tropospheric Emission Monitoring Internet Service), for example.

5.1.2 Total and tropospheric NO_2 column

NO_2 plays a key role in air quality and atmospheric chemistry. It is an air pollutant affecting human health and ecosystems, and an important ozone precursor. In addition, NO_2 is involved in ozone depletion processes in the stratosphere and it is important for climate change studies, because of the indirect effect on the global climate. Total NO_2 columns, including a tropospheric and stratospheric component, are retrieved with the DOAS method in the VIS wavelength region 425–450 nm (Valks et al., 2011). To obtain the stratospheric NO_2 component from the total NO_2 column, a spatial filtering approach is used. After the stratosphere-troposphere separation, the tropospheric NO_2 column is calculated using tropospheric air mass factors based on monthly average NO_2 profiles from the MOZART-2 chemistry transport model. Figure 5 shows the average tropospheric NO_2 columns over East Asia measured by GOME-2A for the

AMTD
8, 6993–7056, 2015

period 2007–2013. The world's largest area with high NO_2 pollution is found above eastern China, which is a result of China's spectacular economic growth during the last decade, accompanied by a strong increase in emissions of air pollutants. Another remarkable feature visible in Fig. 5 is the enhanced tropospheric NO_2 along shipping lanes in the Bay of Bengal and the South China Sea, like in Richter et al. (2011). The GOME-2 tropospheric NO_2 columns are used in the MACC-II NRT system and in support of regional (e.g. European) air quality models, for example. The NO_2 products from the O3M-SAF are also used by a number of research institutes for various applications such as verification of emissions, investigation of regional and global trends, and assessment of chemistry-transport models.

The near real-time and offline total and tropospheric NO_2 products are regularly validated and monitored by comparing to: (1) data sets acquired by other satellites (GOME, SCIAMACHY, OMI) and GOME-2 retrievals performed with other processors (such as the TEMIS system, http://www.temis.nl) and (2) ground-based reference measurements acquired by UV-visible DOAS spectrometers performing network operation in the framework of the Network for the Detection of Atmospheric Composition Change (NDACC, http://ndacc.org) and zenith-sky looking spectrometers for the NO_2 stratospheric column and multi-axis (MAX-DOAS) spectrometers for the NO_2 tropospheric column. Detailed validation results for GOME-2A can be found in Valks et al. (2011). The dedicated O3M SAF BIRA-IASB validation website (http://cdop.aeronomie.be/validation) gathers the latest validation results.

The step by-step verification of the operational GOME-2B product against GOME-2A, and GOME-2A and B alternative retrievals, has highlighted a global underestimation by GOME-2B slant columns of 1×10^{15} molec cm^{-2} with respect to GOME-2A, which translates into a bias of 0.15×10^{15} and 0.4×10^{15} molec cm^{-2} in total and stratospheric columns. GOME-2B tropospheric column data underestimate GOME-2A by less than 0.5×10^{15} molec cm^{-2} in moderately polluted conditions, while larger differences (up to 8×10^{15} molec cm^{-2}) occur in polluted regions. The latter can be explained by the local time difference between GOME-2A and GOME-2B overpasses and the as-

AMTD
8, 6993–7056, 2015

sociated impact of the variability in NO_2 content and cloud cover on the comparison results. Figure 6 presents, from pole to pole, the median bias and spread for total NO_2 between GOME-2A/B total NO_2 and correlative ground-based measurements acquired by 25 zenith-sky DOAS instruments. Prior to the comparisons, GOME-2/NDACC co-located data are filtered to avoid GOME-2 data contaminated by tropospheric pollution, and corrected for photochemical diurnal effects (arising from solar local time differences between NDACC and Metop observations). Only the latest, consolidated versions of the NDACC data are considered for Fig. 6 (no NRT data), and only the GOME-2 forward pixels (no backward pixels). Figure 6 illustrates the good agreement between the different stratospheric NO_2 data sets, usually within $0.1–0.5 \times 10^{14}$ molec cm^{-2}, a value close to the combined uncertainty of the comparison method. Nevertheless, the slight bias between GOME-2A and GOME-2B data is also seen, GOME-2B underestimating GOME-2A by about $1–3 \times 10^{14}$ molec cm^{-2} (bias propagated from the retrieval of slant columns densities), as well as another slight bias of $2–5 \times 10^{14}$ molec cm^{-2} between comparison results averaged over the Northern Hemisphere and those averaged over the Southern Hemisphere.

Figure 7 presents some examples of validation results for tropospheric NO_2 GOME-2 columns based on BIRA-IASB MAXDOAS stations. As can be seen in Fig. 7a, very different conditions of tropospheric NO_2 are sampled at the four stations, from clean/remote region (OHP, south of France), city (Uccle, Belgium) and heavily polluted region in Beijing and Xianghe in China (just outside the city, at 60 km south-east of Beijing). Figure 7b present the scatter plots of the monthly means at the four stations. Good correlations between GOME-2A and the ground-based MAXDOAS data are obtained, both in terms of correlation coefficients R (ranging from 0.65 in Uccle to 0.92 in Beijing) and slopes of the regression analysis S, with values 0.8 at Xianghe, slightly smaller in Uccle and OHP (0.6) and with larger differences ($S = 0.47$) in Beijing. The impact of the location of the ground-based instrument can be seen when comparing the results between Beijing and Xianghe, that are only 60 km apart: in the first case the MAXDOAS is situated in the center of the Beijing megacity and then it has been

AMTD
8, 6993–7056, 2015

moved to the Xianghe site outside the city, in a zone more representative of what seen by a satellite pixel. This "urban effect" has been also highlighted in larger scale comparisons started in Pinardi et al. (2014) for total, stratospheric and tropospheric GOME-2 NO_2 columns compared to DirectSun, ZenithSky and MAXDOAS datasets. Figure 7c presents an example of the time-series of GOME-2A and B above OHP and its comparisons to ground-based MAXDOAS tropospheric NO_2 data, extending the results presented in Valks et al. (2011). The pollution episodes are well captured by both GOME-2 instruments and the comparisons of monthly averaged columns show consistent seasonal variations, with high NO_2 in winter and low NO_2 in summer.

5.1.3 Total H_2CO column

Atmospheric formaldehyde (H_2CO) is an intermediate product common to the degradation of many volatile organic compounds and therefore it is a central component of tropospheric chemistry. While the global formaldehyde background is due to methane oxidation, emissions of non-methane volatile organic compounds (NMVOCs) from biogenic, biomass burning and anthropogenic continental sources result in important and localized enhancements of the H_2CO concentration. Improving our knowledge of NMVOC emissions is essential for a better understanding of the processes that control the production and the evolution of tropospheric ozone, a key actor in air quality and climate change, but also of the hydroxyl radical OH, the main cleansing agent of our troposphere. As the lifetime of H_2CO is typically a few hours, enhanced concentrations serve as tracer for reactive NMVOC emissions (Fig. 8). Moreover, H_2CO satellite observations are used in combination with tropospheric chemistry transport models to constrain NMVOC emission inventories in so-called top-down inversion approaches. Satellite H_2CO and NO_2 observations are also combined to estimate VOC/NO_x ratios, and thereby the local chemical regime of tropospheric ozone production. The main user of the O3M SAF NRT and reprocessed GOME-2 H_2CO products is the MACC-II Copernicus Atmosphere Monitoring Service. The H_2CO retrieval is based on the DOAS technique and follows the developments published in De Smedt et al. (2012).

AMTD
8, 6993–7056, 2015

Common settings are used for GOME-2A and GOME-2B retrievals. The H_2CO slant column inversion is performed in the UV wavelength range 328.5–346 nm, and includes a post-treatment for systematic biases based on a latitude dependent offset correction. Tropospheric H_2CO vertical columns are calculated using air mass factors that depend on the solar and viewing geometries, the surface albedo, cloud fraction and cloud top height (OCRA/ROCINN product), and the H_2CO profile shape which is derived from 3-dimensional chemical-transport model simulations obtained using the IMAGES model (Stavrakou et al., 2009).

For the validation of the H_2CO columns a step-by-step verification of the operational product against the reference scientific GOME-2 H_2CO retrieval algorithm (De Smedt et al., 2012) has been performed. An example of this verification is given in Fig. 9 for two different emissions regions: Northern China and Amazonia. GOME-2B H_2CO slant columns, fit residuals, and scatter are comparable to those obtained from GOME-2A spectra at the beginning of the mission in 2007, both for the operational and scientific products. The effect of Metop-A degradation (increase of the DOAS fit RMS with time) is clearly visible. Differences between operational and scientific datasets are within 40 and 28 % for Metop-A since 2007 and within 20 and 13 % for Metop-B since December 2012, for Amazonia and Northern China respectively. GOME-2 A and B GDP 4.7 H_2CO retrievals are in very good agreement with the reference scientific retrievals when using the same settings (not shown here). The reduced H_2CO slant column noise level in the scientific algorithm presented here (v14) is obtained by pre-fitting BrO in a separate larger interval (328.5–359 nm) which allows decorrelation of H_2CO and BrO differential absorption structures (De Smedt et al., 2012). Remaining differences between the operational and scientific H_2CO vertical columns are mainly related to the different input parameters used for the air mass factor calculation, namely the cloud product and the surface albedo. An improved version of the H_2CO operational product addressing both GOME-2 A and B is under preparation based on recent scientific algorithm developments and will be released with the next version of the GDP data product (GDP 4.8). In addition to the verification against the scientific prototype, comparisons with

AMTD
8, 6993–7056, 2015

other H_2CO satellite datasets, such as GOME, SCIAMACHY and OMI instruments as well as direct comparisons with ground-based MAXDOAS and/or FTIR instruments are planned to be performed in a near future.

5.1.4 Total SO_2 column

Volcanic SO_2 measurements from satellites provide critical information for aviation hazard mitigation and early warning of volcanic unrest. In several regions (e.g. South-East Asia), SO_2 is an important air pollutant affecting human health and ecosystems, and it is responsible for the production of acid rain. Furthermore, sulfate aerosol is important for climate monitoring, since it affects the Earth's radiative balance by scattering incident sunlight back to space. The global SO_2 emissions are shown in the Fig. 10.

The DOAS slant column retrieval of SO_2 is performed in the UV wavelength range 315–326 nm (Rix et al., 2012). The retrieved SO_2 slant columns are corrected for any systematic bias by applying a latitude and surface-elevation dependent offset correction. Total vertical SO_2 columns are calculated by applying an air mass factor which is depending on the viewing geometry surface conditions, and the SO_2 profile shape. Since at the time of the measurement the SO_2 plume height is unknown, the total vertical column is calculated for three scenarios representing the passive degassing of volcanoes and anthropogenic pollution (plume height: 2.5 km); passive degassing of high altitude volcanoes and weak eruptions (6 km); and explosive volcanic eruptions (15 km). Furthermore, in order to detect volcanic eruptions, pixels with elevated SO_2 columns are automatically flagged when they fulfill certain threshold criteria (Brenot et al., 2014). This is especially important for the assimilation of the GOME-2 SO_2 columns in forecast models, such as in the MACC-II system. The main users of the GOME-2 SO_2 product are the volcanic hazard and air quality communities. The GOME-2 SO_2 product is used within the Support to Aviation Control Service (SACS) (Brenot et al., 2014), that provides volcanic plume information to the Volcanic Ash Advisory Centers (VAACs) and other users. The GOME-2 SO_2 columns are also used within the GMES service EVOSS, which monitors volcanic activity and relevant hazard at a global

AMTD
8, 6993–7056, 2015

scale using Earth Observation data products. Furthermore, the GOME-2 SO_2 columns have been used within the mobile volcano fast response system Exupéy (Rix et al., 2009).

The validation of GOME-2 SO_2 columns currently relies on inter-comparisons with other satellite datasets, such as SCIAMACHY/Envisat and OMI/Aura as well as inter-evaluation between the two GOME-2 instruments on Metop platforms. An example of inter-comparison of GOME-2A and GOME-2B for the Copahue volcanic eruption on the 23 December 2012 is given in Fig. 11, left, showing very consistent results between the two sensors for their co-located measurements. Figure 11, right, shows an example of anthropogenic SO_2 comparisons, for a region in Eastern China centralized over Beijing. The OMI/Aura PBL product, which assumes an SO_2 loading with a center of mass altitude of about 0.9 km (Krotkov et al., 2006), is compared to both GOME-2A and GOME-2B observations considering an SO_2 plume height at 2.5 km. A very good correlation between between GOME-2A and B results is shown in the scatter plot (blue line) with r squared of 0.74, to be expected since the same algorithm is applied to both sensors. However, the GOME-2B retrievals result in lower SO_2 columns than the OMI retrievals for loadings over 0.5 DU as shown in the equivalent scatter plot (red line) even though the absolute correlation is very satisfactory at 0.80. The reason for this difference may be attributed to the different assumptions on the a-priori SO_2 profile used by the two different algorithms (see Theys et al., 2013b for more details). In the future, comparisons with ground-based MAXDOAS instruments at different global locations is envisaged for strong anthropogenic and volcanic SO_2 cases as this type of comparison allows the dependence of the retrievals on the SO_2 profile shape to be taken into account.

5.1.5 Total BrO column

BrO is present in the lower stratosphere, where it depletes ozone through very efficient catalytic reactions. BrO is also released in the troposphere from sea ice, at the interface of ocean, salt lakes and volcanoes.

AMTD
8, 6993–7056, 2015

The retrieval of total BrO is achieved by a DOAS analysis in the wavelength region 332–359 nm (Theys et al., 2011), including five BrO absorption bands. It is followed by an equatorial offset correction (Richter et al., 2002) applied to the retrieved slant columns, in order to minimize the impact of the long-term instrumental degradation. The conversion into total BrO vertical columns is made using air mass factors assuming representative stratospheric BrO profiles. The scientific community is using the GOME-2 total BrO product provided by the O3M SAF. The main interest is on bromine emissions in the polar boundary layer. GOME-2 measurements allow springtime BrO columns to be studied in both the Arctic and Antarctic regions (as illustrated in Fig. 12). BrO production is related to heterogeneous photochemistry due to the presence of sea salt, but the mechanisms are currently not fully characterized, especially the link with meterological variables (e.g., wind) and the importance of bromine for the deposition of mercury which impacts the polar biosphere. Owing to its wide coverage, GOME-2 measurements enable long-range transport of polar tropospheric BrO (Begoin et al., 2010) to be studied, and also emissions from volcanic eruptions (Theys et al., 2009a; Hörmann et al., 2013). In addition there is an interest in the study of stratospheric BrO and its long-term trend. However, strictly speaking, scientific studies of BrO from GOME-2 measurements are only possible by separating the retrieved total BrO column into its tropospheric and stratospheric components (see Sect. 6).

The validation of BrO columns relies on the comparison of the total columns to other satellite datasets, such as the SCIAMACHY and GOME-2 scientific products (Theys et al., 2011) and on ground-based zenith-sky DOAS instruments from NDACC stations, such as Harestua (Hendrick et al., 2007). The results for the validation of GOME-2A and B BrO total columns can be found in Theys et al. (2013a) and on the O3M SAF BIRA validation pages (http://cdop.aeronomie.be/validation/valid-results). Examples are shown in Fig. 13. One can see that the satellite columns are very consistent with each other at all latitudes and season. The comparison of GOME-2A and GOME-2B with ground-based BrO columns at Harestua is good as well for the absolute values and for the short-term variation of the BrO total column. The conclusion is that the

AMTD
8, 6993–7056, 2015

GOME-2A and -B total BrO columns have an accuracy better than 30 % most of the time and hence the product reaches its target accuracy.

5.1.6 Total water vapour column

Atmospheric water vapour plays a major role for both meteorological phenomena and climate via its influence on the formation of clouds and precipitation, the growth of aerosols and significantly contributes to the energy balance of the Earth acting as a powerful greenhouse gas. Hence, advancing in understanding of variability and long/term changes in water vapour is vital, especially considering that atmospheric water vapour exhibits a highly variable spatial and temporal distribution. Total column water vapour (TCWV) from GOME-2 is the only data product with the following combination of features: global coverage over land and over sea, good sensitivity down to the surface (where most of the water vapour column resides), independent of model input (no model-dependent information in climatological data record), and retrievals insensitive to instrument drift. Thus, the GOME-2 water vapour product is especially valuable for long-term series and climatological studies (Wagner et al., 2006; Lang et al., 2007; Noël et al., 2008; Mieruch et al., 2010). The example of the retrieved monthly mean maps of total column water vapour in Fig. 14 shows the global distribution of TCWV in February and August 2008 retrieved by GOME-2A. The algorithm used for the retrieval of GOME-2 TCWV is based on a classical Differential Optical Absorption Spectroscopy (DOAS) performed in the wavelength interval 614.0–683.2 nm and does not include explicit numerical modelling of the atmospheric radiative transfer (Wagner et al., 2006; Grossi et al., 2014). It consists of three basic steps: in the first step, the spectral DOAS fitting is carried out, taking into account absorption by O_2 and O_4, in addition to that of water vapour. In the second step, a correction for absorption non-linearity effects is applied because the highly fine structured H_2O (and O_2) absorption bands cannot be spectroscopically resolved by the GOME-2 instrument. In the last step, the corrected water vapour slant columns determined with the DOAS fitting are converted to geometry-independent Vertical Column Densities (VCDs) through divi-

AMTD
8, 6993–7056, 2015

sion by an appropriate Air Mass Factor (AMF), which is derived from the measured O_2 absorption.

To assess the quality of the GOME-2 water vapour columns, the TCWV products were compared with corresponding model data from the European Centre for Medium Range Weather Forecast (ECMWF) ERA-Interim reanalysis (Dee et al., 2011) and with SSMIS satellite F16 measurements (Wentz and Meissner, 2007) during the full period January 2007–June 2014 (Grossi et al., 2014). A comparison between the GOME-2A product and the combined SSM/I + MERIS GlobVapour data set in 2007 and 2008 was also carried out. Good general agreement was reported between all three datasets with mean bias within 0.035 g cm^{-2}, although some seasonal and regional biases have been identified. Figure 15 shows a time series of globally averaged total bias in the TCWV distribution between GOME-2A and the data sets described above. Since January 2013, the bias between the most recent GOME-2B results and the ERA-Interim and SSMIS retrievals was also computed. It was found that the combined SSM/I-MERIS sample and the ERA-Interim data set are typically drier than the GOME-2 retrievals (0.03 and 0.035 g cm^{-2}, respectively), while on average GOME-2 data overestimate the SSMIS measurements by only 0.006 g cm^{-2}. However, the size of these biases is seasonally dependent. Monthly average differences as large as 0.1 g cm^{-2} were observed in the analysis against SSMIS measurements, but were not so evident in the comparison with ERA/Interim and SSM/I + MERIS data, because of the compensating effect of having land and ocean retrievals. Pronounced negative biases over land areas were identified in regions with high humidity or a relatively large surface albedo (0.3–0.5).

The water vapour product has also been validated against ground-based data (Kalakoski et al., 2014). In that study, the radiosonde data were from the Integrated Global Radiosonde Archive (IGRA) maintained by National Climatic Data Center (NCDC) and screened for soundings with incomplete tropospheric column whereas the ground-based GPS observations from COSMIC/SuomiNet network were used as the second independent data source. The outcome described in the paper was that

AMTD
8, 6993–7056, 2015

the general agreement between GOME-2 and the ground-based observations is good. The median relative difference to radiosonde observations was found to be −2.7 % for GOME-2A and −0.3 % for GOME-2B. Against GPS observations, the median relative differences were 4.9 and 3.2 % for GOME-2A and B, respectively. For water vapour total columns below 10 kg m^{-2}, large wet biases were observed, especially against GPS observations. Conversely, at values above 50 kg m^{-2}, GOME-2 generally underestimates both ground-based observations.

5.2 Vertical ozone profiles

The NRT and offline vertical ozone profile product (van Peet et al., 2009, 2014) uses reflectance measurements from 260 to 330 nm and iteratively finds the ozone profile best matching the original radiance measurements using optimal estimation. The ozone profiles are given as partial ozone columns in DU in 40 logarithmically spaced layers from the surface up to 0.001 hPa. For (partially) cloudy scenes, the retrieved cloud pressure replaces the nearest pressure level. The cloud pressure is retrieved by the FRESCO algorithm from the O_2 A-band measurement of GOME-2 (Wang et al., 2008). GOME-2 has nominal spatial resolution of 80 km × 40 km, but for the shortest UV wavelengths the integration time is 8 times longer. The initial O3M SAF ozone profile product was provided at a spatial resolution of 640 km × 40 km (coarse resolution, CR) but has since been improved to the 80 km × 40 km resolution using radiance measurements from a mix of integration times. As an example of the ozone profile product from GOME-2B, Fig. 16 shows a vertical cross section along an orbit from north to south. The measurements end in a location over Antarctica where the Southern Hemisphere spring ozone hole is present, indicated by low ozone values in the stratosphere.

The ozone profile products are validated with ozone sonde data as well as with lidar and microwave measurements. The ozone sonde data are used in particular for the tropospheric and the lower stratospheric part up to about 30 km, whereas lidar and microwave validation focus on the stratosphere from 15 to 55 km. The ozone sonde data comes from the World Ozone and Ultraviolet Data Center (WOUDC), the SHADOZ

AMTD
8, 6993–7056, 2015

(Southern Hemisphere ADditional OZonesondes) network, NDACC (Network for the Detection of Atmospheric Composition Change) and the NILU's Atmospheric Database for Interactive Retrieval (NADIR) at Norsk Institutt for Luftforskning (NILU) (http://www.nilu.no/nadir/). The NDACC network also provides the data of 4 lidar and 5 microwave stations. These are the only NDACC stations which deliver ozone profile data regularly and with comparatively small delay in time. A comprehensive description of the ground based validation methods and results for the upper stratosphere will soon be published elsewhere.

The validation and quality monitoring is done by trending of monthly mean values and by direct comparison of satellite and ground-based data. The regular validation uses ground based ozone profile measurements and considers the dependence of the deviations between satellite and ground based profiles on total ozone, scan angle, solar zenith angle, cloud fraction and distance in space and time. All comparisons are performed for the high and coarse resolution satellite profiles, respectively. The complete set of results is regularly available at the O3M SAF validation internet site.

Overall target values are met in the troposphere (30 %) and the lower stratosphere (15 %), not taking into account the UTLS zone, which shows more elevated relative differences, which cannot be assigned to the troposphere or to the stratosphere. However, GOME-2 shows a clear underestimation of ozone concentrations above about 30 km (Fig. 17). The difference to ground based data increases with altitude, amounting up to about 25 % at 55 km for GOME-2B and up to about 55 % for GOME-2A, depending to some degree on ground based station and instrument. Furthermore, a satellite to satellite comparison with Global Ozone Monitoring by Occultation of Stars (GOMOS), Optical Spectrograph and Infrared Imager System (OSIRIS) and Microwave Limb Sounder (MLS) confirms these conclusions (Määttä et al., 2015).

Degradation of the GOME-2A instrument is clearly visible in the ozone profile products as a decrease in retrieved tropospheric ozone concentrations at most altitudes over the years of the mission (Fig. 18). Especially for the higher stratospheric part (25–30 km), a decrease in retrieved ozone concentrations over the years of the mission for

AMTD
8, 6993–7056, 2015

GOME-2A could be identified. For the coarse resolution profiles, this trend can be as large as 75 % per decade in the upper stratosphere above 30 km. GOME-2B data (red lines in Fig. 18) don't show this effect yet. Thus, the implementation of the degradation correction is an important part of the algorithm development in future.

5.3 Aerosol products

The Absorbing Aerosol Index (AAI) product is derived from the reflectances measured by GOME-2 at 340 and 380 nm (Tilstra et al., 2010). The AAI may be used to detect absorbing aerosols over both land and sea surfaces, even in the presence of clouds. The AAI retrieval algorithm compares the measured reflectances with simulated clear-sky reflectances and calculates a "residue" from these which represents the difference between measurement and (clear-sky) simulation and takes the form of a single index.

In the algorithm, the surface albedo is assumed to be constant over the spectral range of the two selected wavelengths, and when the total ozone column is taken into account in the simulations, deviations from the Rayleigh scattering atmosphere are caused purely by clouds and/or aerosols. Negative values for the AAI are caused by the presence of clouds and/or scattering aerosol in the scene. However, a positive value for the AAI can only be explained by the presence of absorbing aerosols. This makes the AAI ideally suited for aerosol masking and the detection of smoke from forest fires or volcanic eruptions. An example of the detection of a volcanic plume is shown in Fig. 19, where the ash plume originating from the Puyehue volcano can be seen to travel from its source eastward over the south Atlantic Ocean. This event has been analyzed in Wang et al. (2012).

For the validation of the GOME-2 AAI product we rely on comparisons with AAI products derived from other satellite instruments, such as GOME-1, SCIAMACHY and OMI. The validation results show that the GOME-2 AAI has reached the target accuracy of 0.5 index point (Tilstra et al., 2013).

AMTD
8, 6993–7056, 2015

5.4 Lambertian-equivalent reflectivity surface albedo database

The Lambertian-equivalent reflectivity (LER) of the Earth's surface is based on reflectance measurements taken by GOME-2 on the Metop-A satellite. It is the improved follow-up of earlier surface LER databases based on GOME-1 (on the ERS-2 satellite) and OMI (on the Aura satellite). The surface LER is an essential input parameter for the retrieval of many trace gases, clouds properties, and aerosols.

The GOME-2 surface LER is retrieved from the main science channels for 15 predefined one-nm wide wavelength bands ranging from the UV to the near-infrared. Additionally, we provide a surface LER product based on the PMD (Polarization Measurement Device) measurements. The definition of these PMD bands is fixed but the advantage is the much smaller footprint size (10 km × 40 km instead of 80 km × 40 km) which results in better statistics. The surface LER spectra are provided for each month of the year in a grid of 1° × 1° (MSC-LER) or 0.5° × 0.5° (PMD-LER).

The retrieval algorithm follows an approach in which the reflectance measurements from the entire mission are transformed for each of the months into scene LERs. The scene LERs are distributed into the grid cells of the Earth grid and their histograms are analyzed to find the representative (cloud-free) scene LER, i.e., the spectral surface LER. For some surfaces the mode of this distribution is taken (e.g. snow, desert), for others the minimum value is taken (e.g. ocean). Cloud contamination over the oceans caused by persistent cloud presence is corrected by looking for near-by grid cells that can act as a surface LER donor. The surface LER is retrieved for land and sea surfaces, including those covered by snow and ice. A more extensive description of the algorithm and product can be found in Tilstra et al. (2014). An example of the surface LER product is presented in Fig. 20.

5.5 UV radiation products

Offline surface ultraviolet (UV) radiation products (OUV) contain the most important quantities of the solar radiation that can be harmful to life and materials on the Earth.

AMTD
8, 6993–7056, 2015

These quantities include daily doses and maximum dose rates of integrated UVB and UVA radiation together with values obtained by different biological weighting functions, solar noon UV Index and quality control flags. Recent additions are the photolysis frequencies of two key reactions in the atmospheric chemistry of the troposphere: the photodissociation of ozone and nitrogen dioxide. The photolysis frequency of ozone refers to the rate constant $j_{O(^1D)}$ of the following reaction forming atomic oxygen in its exited ^{1}D state from ozone

$$O_3 + h\nu(\lambda<320\,\text{nm}) \rightarrow O(^1D) + O_2 \quad \text{(R1)}$$

This is an important photodissociation route of ozone leading to production of the hydroxyl radical, a key species in oxidation of hydrocarbons in the troposphere. Figure 21 shows, as an example, the daily maximum $j_{O(^1D)}$ at ground level on 10 April 2015.

The OUV products are derived from the O3M SAF total ozone column product and the visible channel reflectances of the third Advanced Very High Resolution Radiometer (AVHRR/3), therefore combining data from two different instruments aboard the Metop satellites (Kujanpää and Kalakoski, 2015). Sampling of the diurnal cloud cycle is improved by complementing the morning orbit Metop AVHRR/3 data with corresponding afternoon orbit data from the Polar Orbiting Environmental Satellites (POES) of the National Oceanic and Atmospheric Administration (NOAA), available through the data exchange between EUMETSAT and NOAA in their Initial Joint Polar System (IJPS) programme. The validation results will be presented in a paper by Kalakoski and Kujanpää (2015). The offline UV products are currently used by research institutes in Europe and Australia.

The Near Real Time UV product is a 1–5 day forecast of UV index on global scale. The NUV/CLEAR product is based on GOME-2 assimilated total ozone (ATO) from KNMI. UV index is calculated from ATO applying climatologies for surface albedo, aerosol optical depth etc. The final NUV/CLEAR index is valid for clear-sky conditions at local noon, i.e. minimum solar zenith angle, thus reflecting the maximum UV index to be expected for the current day. The NUV/CLOUD product is the NUV/CLEAR prod-

AMTD
8, 6993–7056, 2015

uct modified with an algorithm using the cloud cover fraction forecast from ECMWF to reflect the actual UV index. The UV fields are calculated on the same grid size as the input ATO fields, with a sub-pixel resolution of 0.25° × 0.25°. The product may be highly customized for users, with regard to geographical coverage, forecast time etc.

The NUV/CLEAR and NUV/CLOUD have been validated against ground-based measurements of UV index. The most recent validation was performed on data from 2011 for 6 locations with a total of 2064 measurements. In Fig. 22 the distribution of the difference between measured and forecasted NUV/CLOUD product is shown. The red line is the mean and the blue line the median of the distribution. The mean absolute relative difference is 22.6 % for the whole NUV/CLOUD comparison, while the NUV/CLEAR product shows a mean absolute relative difference of 8.5 %.

6 Emerging products

The existing O3M SAF GOME-2 L2 products will be reprocessed in 2015. The reprocessed trace gas products as well as aerosol products will be available in fall 2015 whereas the reprocessed OUV products will be available in late 2015.

The O3M SAF project will release completely new GOME-2 products within next two years. The products will be: tropospheric ozone, tropospheric BrO, Glyoxal (CHOCHO), OClO and monthly climate products of H_2O and NO_2. The products are described below.

There will be two different kinds of tropospheric ozone products. The first one will be a product called Tropical Tropospheric Ozone Columns (TTOCs) using a convective-cloud-differential (CCD) method (Valks et al., 2014). The retrieval is based on total ozone and cloud property data provided by the GDP 4.8 (see Sect. 3.1), and uses above-cloud and clear-sky ozone column measurements to derive a monthly mean TOC between 20° N and 20° S. Tropical tropospheric ozone data from GOME-2 will provide significant input for climate services and international assessment reports, such as the UNEP/WMO Scientific Assessments of Ozone Depletion and the Climate As-

AMTD
8, 6993–7056, 2015

sessment Reports of IPCC. The second tropospheric ozone product will be based on the separation of the tropospheric and stratospheric columns from the retrieved vertical ozone profiles by splitting the atmosphere at the tropopause and adding the partial ozone columns below and above it. The definition of the tropopause height is a crucial for this product. The World Meteorological Organization defines it as the lowest level at which the lapse rate decreases to 2 C km^{-1} or less, provided that the average lapse rate between this level and all higher levels within 2 km does not exceed 2 C km^{-1} (WMO Manual on Codes, Vol.I.1-A, WMO-No. 306). However, the tropopause may be defined also just by using a fixed pressure level. If the interest is at the near ground levels, the latter is simpler and more robust approach. Both of these tropospheric ozone products will be available in about mid 2015.

Satellite total BrO columns sometimes exhibit strong stratospheric enhancements of BrO, making the interpretation of the results difficult (Theys et al., 2009b; Salawitch et al., 2010). In the frame of the O3M SAF, it is planned to produce tropospheric BrO columns following the approach developed by Theys et al. (2011) The retrieval of tropospheric BrO columns is achieved through a stratospheric correction based on a BrO climatology that accounts for the important dynamical and photochemical variations of stratospheric BrO (Theys et al., 2009b). The algorithm treats also the changes in sensitivity in both tropospheric and stratospheric layers. By separating the large-scale BrO structures (of tropospheric or stratospheric origin) in the total BrO field, the method allows the polar emissions hotspots and global free-tropospheric BrO background to be better studied.

Glyoxal (CHOCHO) is a short-lived volatile organic compound (VOC) produced in the atmosphere mostly via the oxidation of other non-methane VOCs emitted by natural and human activities, but also directly emitted by fire events and combustion processes (Fu et al., 2008; Stavrakou et al., 2009). Observations of glyoxal atmospheric concentrations are therefore useful to further constrain estimates of VOC emissions and also to improve the global budget of secondary organic aerosols, for which it has been recognized as an important source (Hallquist et al., 2009). Glyoxal has three ab-

AMTD
8, 6993–7056, 2015

sorption bands ranging between 420 and 460 nm, which may be exploited for detection based on the DOAS technique. It has been observed for the first time from space by the SCIAMACHY instrument aboard Envisat (Wittrock et al., 2006). Since then, the GOME-2A data have also been used to retrieve glyoxal tropospheric columns by different teams (Lerot et al., 2010; Vrekoussis et al., 2010). Glyoxal retrievals from space are particularly challenging owing to the weakness of its typical atmospheric optical depth, which leads to strong interferences with other species absorbing in this spectral range. In particular, significant spectral interferences occur with liquid water absorption over remote oceanic areas. Lerot et al. (2010) designed an original 2-step fit method to limit the impact of these interferences. This scientific algorithm will be used as the baseline for implementing an operational tropospheric glyoxal product as part of the O3M-SAF activities in the next two years.

The OClO slant column (in molec cm^{-2}) measurements will be available under chlorine activated ozone hole conditions. Retrieval is only possible under twilight conditions because this molecule is destroyed in full daylight. The algorithm is based on the classical DOAS method. Slant columns of OClO are derived from the differential absorption structures in a spectral region from 365 to 389 nm.

Climate products: data sets of H_2O and NO_2 will consist of monthly mean averages of GOME-2 products in the netCDF format. These will be available in early 2016.

7 Dissemination channels and methods

The main distribution channel for the NRT data is EUMETCast, utilizing the Eurobird-9 satellite. EUMETCast is a multi-service dissemination system based on standard Digital Video Broadcast (DVB) technology and uses commercial telecommunication geostationary satellites to multi-cast files (data and products) to a wide user community. The channel SAF-Europe transmits nearly all products in HDF5 format and channel SAF-Africa transmits trace gas as HDF5 and ozone profile products in BUFR format. Furthermore, trace gas column and ozone profile products are available in BUFR for-

AMTD
8, 6993–7056, 2015

mat via WMO GTS (Global Telecommunication System). The GTS bulletin headers are presented in Table 3. The trace gas products may be obtained also by using the FTP services and in the case of NRT UV via dedicated DMI webpage (http://nuv.dmi.dk/), FTP and Google Earth (http://o3msaf.fmi.fi/products/nuv.kml). All retrieval options with instructions are available from the O3M SAF WWW service (http://o3msaf.fmi.fi/). The timeliness requirement for the NRT products is three hours from sensing.

The offline products as well as long-term data records are available in HDF5 format from data archives hosted by FMI and DLR. Both of these archives are accessible via registration and data ordering service that is available in the O3M SAF main WWW site (http://o3msaf.fmi.fi/). Furthermore, the offline data are also available using the EUMETSAT Earth Observation Portal (https://eoportal.eumetsat.int/). The timeliness requirement for the offline products is two weeks from sensing. The data is free of charge. However, the registration is a mandatory step when retrieving data for the first time.

The daily updated example images of the O3M SAF products are available from the O3M SAF WWW site. Furthermore, images of several O3M SAF GOME-2 products are also available on the TEMIS scientific data portal (www.temis.nl), where GOME-2 data can be compared and combined with data from GOME, SCIAMACHY and OMI.

Beside broadcast dissemination (EUMETCast and WMO/GTS) and FTP/http downloads, the O3M-SAF provides web mapping services for trace gas data in three distinct timeliness categories: latest NRT data of today updated every 15 min, NRT data of yesterday and mission-lifetime time series of daily offline data. These services have been established and operated by DLR (Heinen et al., 2009) and they comply to the OGC standards Web Mapping Service for visualization and Web Coverage Service for download. The address for the Web Map Service is http://geoservice.dlr.de/eoc/atmosphere/wms?SERVICE=WMS&REQUEST=GetCapabilities and for the Web Coverage Service http://geoservice.dlr.de/eoc/atmosphere/wcs?SERVICE=WCS&REQUEST=GetCapabilities.

AMTD
8, 6993–7056, 2015

The O3M SAF L2 data can be used with BEAT (The Basic Envisat Atmospheric Toolbox) and VISAN (BEAT visualization package). The interfaces and description files are implemented into the BEAT by the S&T company.

8 Discussion

At the time when the first signs of the ozone layer recovery emerge, human-induced air quality problems become more severe, monitoring of international conventions are established and the environmental security issues, like for example for aviation, are realized to be extremely valuable. The need for long-term quality-monitored 24/7 data services is also increasing. The operational systems such as the EUMETSAT distributed ground segments are an important example. The development and modification of such systems may not be the fastest process due to the extensive review and quality monitoring requirements. Furthermore, the need for stability and homogeneity doesn't allow sudden changes. However, the outcome is a well-documented product applying the state-of-the-art algorithms following the most resent research results and reliable data dissemination to the users. Furthermore, user services are provided by the product experts which ensure the correct usage of the products.

The ground system is depending on the instruments and data they provide. The GOME-2 instruments provide a long homogenous data record of fifteen years. Furthermore, they continues the data sets started with the GOME instruments and will be followed by the Sentinel 5 instrument onboard the EPS-SG (EUMETSAT Polar Satellites – Second Generation) platforms. This complete data record is particularly suitable for climate studies, reprocessing as well as trend analysis whereas the current GOME-2 products are used in analysis and forecast modeling as well as monitoring of AQ conventions and natural hazards. The O3M SAF GOME-2 products cover the most important atmospheric constituents and radiation values and thus, the products are used in many operational and scientific applications such as weather forecasting, climatological trend analysis, climatic reanalysis, air quality analysis, UV radiation warnings and

AMTD
8, 6993–7056, 2015

volcanic emission alerts. The accuracy of the products meets the target requirements and only in special conditions, e.g. in the UTLS or with high SZA, the requirements are not fully met. The data is disseminated via several channels for both NRT as well as offline and data record users.

Overall, the O3M SAF GOME-2 products have an important impact on our knowledge of a number of fields of research and monitoring of the atmosphere.

Acknowledgements. The O3M SAF is part of the EUMETSAT Satellite Application Facility Ground Segment. The project is funded by EUMETSAT and involved national entities. Part of the validation results are based on ground-based data acquired in the framework of the Network for the Detection of Atmospheric Composition Change (NDACC) and are available publicly (see http://ndacc.org). Advanced validation methods were developed under EC FP6 GEOMon and BELSPO/ProDEx SECPEA and A3C projects.

References

Begoin, M., Richter, A., Weber, M., Kaleschke, L., Tian-Kunze, X., Stohl, A., Theys, N., and Burrows, J. P.: Satellite observations of long range transport of a large BrO plume in the Arctic, Atmos. Chem. Phys., 10, 6515–6526, doi:10.5194/acp-10-6515-2010, 2010. 7011

Bovensmann, H., Burrows, J. P., Buchwitz, M., Frerick, J., Noel, S., Rozanov, V. V., Chance, K. V., and Goede, A. P. H.: Satellite observations of long range transport of a large BrO plume in the Arctic, J. Atmos. Sci., 56, 127–150, 1999. 6996

Brenot, H., Theys, N., Clarisse, L., van Geffen, J., van Gent, J., Van Roozendael, M., van der A, R., Hurtmans, D., Coheur, P.-F., Clerbaux, C., Valks, P., Hedelt, P., Prata, F., Rasson, O., Sievers, K., and Zehner, C.: Support to Aviation Control Service (SACS): an online service for near-real-time satellite monitoring of volcanic plumes, Nat. Hazards Earth Syst. Sci., 14, 1099–1123, doi:10.5194/nhess-14-1099-2014, 2014. 7009

Burrows, J. P., Chance, K. V., Goede, A. P. H., Guzzi, R., Gerridge, J., Muller, C., Perner, D., Platt, U., Pommerau, J.-P., Scheider, W., Spurr, J., and van der Woerd, H.: Global Ozone Monitoring Experiment, Interim Science Report SP-1151, ESA, 1993. 6998

AMTD
8, 6993–7056, 2015

Callies, J., Corpaccioli, E., Eisinger, M., Hahne, A., and Lefebvre, A.: GOME-2 – Metop's second-generation sensor for operational ozone monitoring, ESA Bull.-Eur. Space, 102, 28–36, 2000. 6996, 6998

De Smedt, I., Van Roozendael, M., Stavrakou, T., Müller, J.-F., Lerot, C., Theys, N., Valks, P., Hao, N., and van der A, R.: Improved retrieval of global tropospheric formaldehyde columns from GOME-2/MetOp-A addressing noise reduction and instrumental degradation issues, Atmos. Meas. Tech., 5, 2933–2949, doi:10.5194/amt-5-2933-2012, 2012. 7007, 7008

Dee, D. P., Uppala, S. M., Simmons, A. J., Berrisford, P., Poli, P., Kobayashi, S., Andrae, U., Balmaseda, M. A., Balsamo, G., Bauer, P., Bechtold, P., Beljaars, A. C. M., van de Berg, L., Bidlot, J., Bormann, N., Delsol, C., Dragani, R., Fuentes, M., Geer, A. J., Haimberger, L., Healy, S. B., Hersbach, H., Hólm, E. V., Isaksen, L., Kållberg, P., Köhler, M., Matricardi, M., McNally, A. P., Monge-Sanz, B. M., Morcrette, J.-J., Park, B.-K., Peubey, C., de Rosnay, P., Tavolato, C., Thaut, J.-N., and Vitart, F.: The ERA-Interim reanalysis: configuration and performance of the data assimilation system, Q. J. Roy. Meteor. Soc., 137, 553–597, doi:10.1002/qj.828, 2011. 7013

Eskes, H., van Velthoven, P., Valks, P., and Kelder, H.: Assimilation of GOME total ozone satellite observations in a three-dimensional tracer transport model, Q. J. Roy. Meteor. Soc., 129, 1663–1681, 2003. 7000

Fu, T., Jacob, D. J., Wittrock, F., Burrows, J. P., Vrekoussis, M., and Henze, D. K.: Global budgets of atmospheric glyoxal and methylglyoxal, and implications for formation of secondary organic aerosols, J. Geophys. Res., 113, D15303, doi:10.1029/2007JD009505, 2008. 7020

Grossi, M., Valks, P., Loyola, D., Aberle, B., Slijkhuis, S., Wagner, T., Beirle, S., and Lang, R.: Total column water vapour measurements from GOME-2 MetOp-A and MetOp-B, Atmos. Meas. Tech., 8, 1111–1133, doi:10.5194/amt-8-1111-2015, 2015. 7012, 7013

Hallquist, M., Wenger, J. C., Baltensperger, U., Rudich, Y., Simpson, D., Claeys, M., Dommen, J., Donahue, N. M., George, C., Goldstein, A. H., Hamilton, J. F., Herrmann, H., Hoffmann, T., Iinuma, Y., Jang, M., Jenkin, M. E., Jimenez, J. L., Kiendler-Scharr, A., Maenhaut, W., McFiggans, G., Mentel, Th. F., Monod, A., Prévôt, A. S. H., Seinfeld, J. H., Surratt, J. D., Szmigielski, R., and Wildt, J.: The formation, properties and impact of secondary organic aerosol: current and emerging issues, Atmos. Chem. Phys., 9, 5155–5236, doi:10.5194/acp-9-5155-2009, 2009. 7020

Hao, N., Koukouli, M. E., Inness, A., Valks, P., Loyola, D. G., Zimmer, W., Balis, D. S., Zyrichidou, I., Van Roozendael, M., Lerot, C., and Spurr, R. J. D.: GOME-2 total ozone columns

AMTD
8, 6993–7056, 2015

from MetOp-A/MetOp-B and assimilation in the MACC system, Atmos. Meas. Tech., 7, 2937–2951, doi:10.5194/amt-7-2937-2014, 2014. 7002, 7003

Heinen, T., Kiemle, S., Buckl, B., Mikusch, E., and Loyola, D.: The geospatial service infrastructure for DLR's national remote sensing data library, IEEE Geosci. Remote S., 2, 260–269, doi:10.1109/JSTARS.2010.2040505, 2009. 7022

Hendrick, F., Van Roozendael, M., Chipperfield, M. P., Dorf, M., Goutail, F., Yang, X., Fayt, C., Hermans, C., Pfeilsticker, K., Pommereau, J.-P., Pyle, J. A., Theys, N., and De Mazière, M.: Retrieval of stratospheric and tropospheric BrO profiles and columns using ground-based zenith-sky DOAS observations at Harestua, 60° N, Atmos. Chem. Phys., 7, 4869–4885, doi:10.5194/acp-7-4869-2007, 2007. 7011

Hörmann, C., Sihler, H., Bobrowski, N., Beirle, S., Penning de Vries, M., Platt, U., and Wagner, T.: Systematic investigation of bromine monoxide in volcanic plumes from space by using the GOME-2 instrument, Atmos. Chem. Phys., 13, 4749–4781, doi:10.5194/acp-13-4749-2013, 2013. 7011

Kalakoski, N. and Kujanpää, J.: Validation of the O3M SAF OUV products, to be submitted to Atmos. Meas. Tech. Discuss., 2015. 7018

Kalakoski, N., Kujanpää, J., Sofieva, V., Tamminen, J., Grossi, M., and Valks, P.: Comparison of GOME-2/Metop total column water vapour with ground-based and in situ measurements, Atmos. Meas. Tech. Discuss., 7, 12517–12543, doi:10.5194/amtd-7-12517-2014, 2014. 7013

Koukouli, M. E., Balis, D. S., Loyola, D., Valks, P., Zimmer, W., Hao, N., Lambert, J.-C., Van Roozendael, M., Lerot, C., and Spurr, R. J. D.: Geophysical validation and long-term consistency between GOME-2/MetOp-A total ozone column and measurements from the sensors GOME/ERS-2, SCIAMACHY/ENVISAT and OMI/Aura, Atmos. Meas. Tech., 5, 2169–2181, doi:10.5194/amt-5-2169-2012, 2012. 7003

Krotkov, N. A., Carn, S. A., Krueger, A. J., Bhartia, P. K., and Yang, K.: Band residual difference algorithm for retrieval of SO_2 from the Aura Ozone Monitoring Instrument (OMI), IEEE T. Geosci. Remote, AURA Special Issue, 44, 1259–1266, doi:10.1109/TGRS.2005.861932, 2006. 7010

Kujanpää, J. and Kalakoski, N.: Operational surface UV radiation product from GOME-2 and AVHRR/3 data, Atmos. Meas. Tech. Discuss., 8, 4537–4580, doi:10.5194/amtd-8-4537-2015, 2015. 7018

AMTD
8, 6993–7056, 2015

Lang, R., Casadio, S., Maurellis, A. N., and Lawrence, M. G.: Evaluation of the GOME Water Vapor Climatology 1995–2002, J. Geophys. Res.-Atmos., 112, D17110, 2156–2202, doi:10.1029/2006JD008246, 2007. 7012

Lerot, C., Stavrakou, T., De Smedt, I., Müller, J.-F., and Van Roozendael, M.: Glyoxal vertical columns from GOME-2 backscattered light measurements and comparisons with a global model, Atmos. Chem. Phys., 10, 12059–12072, doi:10.5194/acp-10-12059-2010, 2010. 7021

Lerot, C., Van Roozendael, M., Spurr, R., Loyola, D., Coldewey-Egbers, M., Kochenova, S., Gent, J., Koukouli, M., Balis, D., Lambert, J.-C., Granville, J., and Zehner, C.: Homogenized total ozone data records from the European sensors GOME/ERS-2, SCIAMACHY/Envisat, and GOME-2/MetOp-A, J. Geophys. Res., 119, 1639–1662, doi:10.1002/2013JD020831, 2014. 7003

Loyola, D. G., Koukouli, M. E., Valks, P., Balis, D. S., Hao, N., Van Roozendael, M., Spurr, R. J. D., Zimmer, W., Kiemle, S., Lerot, C., and Lambert, J.-C.: The GOME-2 total column ozone product: retrieval algorithm and ground-based validation, J. Geophys. Res., 116, D07302, doi:10.1029/2010JD014675, 2011. 7002, 7003

Malicet, J., Daumont, D., Charbonnier, J., Parisse, C., Chakir, A., and Brion, J.: Ozone UV spectroscopy. II. Absorption cross-sections and temperature dependence, J. Atmos. Chem., 21, 263–273, doi:10.1007/BF00696758, 1995. 7003

McPeters, R. D., Bhartia, P. K., Haffner, D., Labow, G. J., and Flynn, L.: The version 8.6 SBUV ozone data record: An overview, J. Geophys. Res., 118, 8032–8039, doi:10.1002/jgrd.50597, 2013. 7003

Mieruch, S., Schröder, M., Noël, S., and Schultz, J.: Comparison of monthly means of global total column water vapor retrieved from independent satellite observations, J. Geophys. Res., 115, D23310, doi:10.1029/2010JD013946, 2010. 7012

Munro, R., Eisinger, M., Anderson, C., Callies, J., Corpaccioli, E., Lang, R., Lefebvre, A., Livschitz, Y., and Albiñana, A. P.: GOME-2 on MetOp, in: Proc. of the 2006 EUMETSAT Meteorological Satellite Conference, Helsinki, Finland, EUMETSAT, 48 pp., 2006. 6996

Munro, R., Lang, R., Klaes, D., Poli, G., Retscher, C., Lindstrot, R., Huckle, R., Lacan, A., Grzegorski, M., Holdak, A., Kokhanovsky, A., Livschitz, J., and Eisinger, M.: The GOME-2 instrument on the Metop series of satellites: instrument design, calibration, and level 1 data processing – an overview, Atmos. Meas. Tech. Discuss., in press, 2015.

AMTD
8, 6993–7056, 2015

Noël, S., Mieruch, S., Bovensmann, H., and Burrows, J. P.: Preliminary results of GOME-2 water vapour retrievals and first applications in polar regions, Atmos. Chem. Phys., 8, 1519–1529, doi:10.5194/acp-8-1519-2008, 2008. 7012

Pinardi, G., Van Roozendael, M., Lambert, J.-C., Granville, J., Hendrick, F., Tack, F., Yu, H., Cede, A., Kanaya, Y., Irie, I., Goutail, F., Pommereau, J.-P., Pazmino, A., Wittrock, F., Richter, A., Wagner, T., Gu, M., Remmers, J., Friess, U., Vlemmix, T., Piters, A., Hao, N., Tiefengraber, M., Herman, J., Abuhassan, N., Bais, A., Kouremeti, N., Hovila, J., Holla, R., Chong, J., Postylyakov, O., and Ma, J.: GOME-2 total and tropospheric NO_2 validation based on zenith-sky, direct-sun and multi-axis DOAS network observations, in: Proc. of the 2014 EUMETSAT Meteorological Satellite Conference, Geneva, Swizerland, EUMETSAT, 2014. 7007

Platt, U. and Stutz, J.: Differential Optical Absorption Spectroscopy: Principles and Applications (Physics of Earth and Space Environments), Springer-Verlag, 2008. 7002

Richter, A., Wittrock, F., Ladstätter-Weissenmayer, A. L., and Burrows, J. P.: GOME measurements of stratospheric and tropospheric BrO, Adv. Space Res., 29, 1667–1672, 2002. 7011

Richter, A., Begoin, M., Hilboll, A., and Burrows, J. P.: An improved NO_2 retrieval for the GOME-2 satellite instrument, Atmos. Meas. Tech., 4, 1147–1159, doi:10.5194/amt-4-1147-2011, 2011. 7005

Rix, M., Valks, P., Hao, N., van Geffen, J., Clerbaux, C., Clarisse, C., Coheur, P.-F., Loyola, D., Erbertseder, T., Zimmer, W., and Emmadi, S.: Satellite monitoring of volcanic sulfur dioxide emissions for early warning of volcanic hazards, IEEE J. Sel. Top. Appl., 2, 196–206, doi:10.1109/JSTARS.2009.2031120, 2009. 7010

Rix, M., Valks, P., Hao, N., Loyola, D., Schlager, H., Huntrieser, H., Flemming, J., Koehler, U., Schumann, U., and Inness, A.: Volcanic SO_2, BrO and plume height estimations using GOME-2 satellite measurements during the eruption of Eyjafjallajökull in May 2010, J. Geophys. Res., 117, D00U19, doi:10.1029/2011JD016718, 2012. 7009

Salawitch, R. J., Canty, T., Kurosu, T., Chance, K., Liang, Q., da Silva, A., Pawson, S., Nielsen, J. E., Rodriguez, J. M., Bhartia, P. K., Liu, X., Huey, L. G., Liao, J., Stickel, R. E., Tanner, D. J., Dibb, J. E., Simpson, W. R., Donohoue, D., Weinheimer, A., Flocke, F., Knapp, D., Montzka, D., Neuman, J. A., Nowak, J. B., Ryerson, T. B., Oltmans, S., Blake, D. R., Atlas, E. L., Kinnison, D. E., Tilmes, S., Pan, L. L., Hendrick, F., Van Roozendael, M., Kreher, K., Johnston, P. V., Gao, R. S., Johnson, B., Bui, T. P., Chen, G., Pierce, R. B., Crawford, J. H.,

AMTD
8, 6993–7056, 2015

and Jacob, D. J.: A new interpretation of total column BrO during Arctic spring, Geophys. Res. Lett., 37, , L21805, doi:10.1029/2010GL043798, 2010. 7020

Stavrakou, T., Müller, J.-F., De Smedt, I., Van Roozendael, M., Kanakidou, M., Vrekoussis, M., Wittrock, F., Richter, A., and Burrows, J. P.: The continental source of glyoxal estimated by the synergistic use of spaceborne measurements and inverse modelling, Atmos. Chem. Phys., 9, 8431–8446, doi:10.5194/acp-9-8431-2009, 2009. 7008, 7020

Theys, N., Van Roozendael, M., Dils, B., Hendrick, F., Hao, N., and De Maziére, M.: First satellite detection of volcanic bromine monoxide emission after the Kasatochi eruption, Geophys. Res. Lett, 36, L03809, doi:10.1029/2008GL036552, 2009a. 7011

Theys, N., Van Roozendael, M., Errera, Q., Hendrick, F., Daerden, F., Chabrillat, S., Dorf, M., Pfeilsticker, K., Rozanov, A., Lotz, W., Burrows, J. P., Lambert, J.-C., Goutail, F., Roscoe, H. K., and De Mazière, M.: A global stratospheric bromine monoxide climatology based on the BASCOE chemical transport model, Atmos. Chem. Phys., 9, 831–848, doi:10.5194/acp-9-831-2009, 2009b. 7020

Theys, N., Van Roozendael, M., Hendrick, F., Yang, X., De Smedt, I., Richter, A., Begoin, M., Errera, Q., Johnston, P. V., Kreher, K., and De Mazière, M.: Global observations of tropospheric BrO columns using GOME-2 satellite data, Atmos. Chem. Phys., 11, 1791–1811, doi:10.5194/acp-11-1791-2011, 2011. 7011, 7020

Theys, N., Hendrick, F., van Roozendael, M., Hao, N., and Valks, P.: Interim verification report of GOME-2 GDP 4.7 BrO column data for MetOp-B Operational Readiness Review, Technical Note/Validation Report SAF/O3M/IASB/VR/BRO/091/TN-IASB-GOME2B-O3MSAF-BRO-2013), O3M SAF, available at: http://o3msaf.fmi.fi/docs/vr/Validation_Report_OTO_BRO_Jun_2013.pdf, 2013a. 7011

Theys, N., Van Gent, J., van Roozendael, M., Koukouli, M., Balis, D., Hedelt, P., and Valks, P.: Interim verification report of GOME-2 GDP 4.7 SO_2 column data for MetOp-B Operational Readiness Review, Technical Note/Validation Report SAF/O3M/IASB/VR/SO2/TN-IASB-GOME2B-O3MSAF-SO2-2013), O3M SAF, available at: http://o3msaf.fmi.fi/docs/vr/Validation_Report_OTO_SO2_May_2013.pdf, 2013b. 7010

Tilstra, L. G., Tuinder, O. N. E., and Stammes, P.: GOME-2 Absorbing Aerosol Index: Statistical analysis, comparison to GOME-1 and impact of instrument degradation, in: Proceedings of the 2010 EUMETSAT Meteorological Satellite Conference, EUMETSAT, iSBN 978-92-9110-089-7, 57 pp., 2010. 7016

AMTD
8, 6993–7056, 2015

Tilstra, L. G., Tuinder, O. N. E., and Stammes, P.: O3M SAF Validation Report for Aerosol Products, Technical Note/Validation Report SAF/O3M/KNMI/VR/001), O3M SAF, available at: http://o3msaf.fmi.fi/docs/vr/Validation_Report_ARS_AAI_Jun_2013.pdf, 2013. 7016

Tilstra, L. G., Tuinder, O. N. E., and Stammes, P.: GOME-2 surface LER product – Algorithm Theoretical Basis Document, ATBD O3MSAF/KNMI/ATBD/003), O3M SAF, available at: http://o3msaf.fmi.fi/docs/atbd/Algorithm_Theoretical_Basis_Document_LER_Nov_2014.pdf, 2014. 7017

Valks, P., Pinardi, G., Richter, A., Lambert, J.-C., Hao, N., Loyola, D., Van Roozendael, M., and Emmadi, S.: Operational total and tropospheric NO_2 column retrieval for GOME-2, Atmos. Meas. Tech., 4, 1491–1514, doi:10.5194/amt-4-1491-2011, 2011. 7004, 7005, 7007

Valks, P., Hao, N., Gimeno Garcia, S., Loyola, D., Dameris, M., Jöckel, P., and Delcloo, A.: Tropical tropospheric ozone column retrieval for GOME-2, Atmos. Meas. Tech., 7, 2513–2530, doi:10.5194/amt-7-2513-2014, 2014. 7019

van Peet, J. C. A., van der A, R. J., de Laat, A. T. J., Tuinder, O. N. E., König-Langlo, G., and Wittig, J.: Height resolved ozone hole structure as observed by the Global Ozone Monitoring Experiment-2, Geophys. Res. Lett., 36, , L11816, doi:10.1029/2009GL038603, 2009. 7014

van Peet, J. C. A., van der A, R. J., Tuinder, O. N. E., Wolfram, E., Salvador, J., Levelt, P. F., and Kelder, H. M.: Ozone ProfilE Retrieval Algorithm (OPERA) for nadir-looking satellite instruments in the UV–VIS, Atmos. Meas. Tech., 7, 859–876, doi:10.5194/amt-7-859-2014, 2014. 7014

Van Roozendael, M., Loyola, D., Spurr, R., Balis, D., Lambert, J.-C., Livschitz, Y., Valks, P., Ruppert, T., Kenter, P., Fayt, C., and Zehner, C.: Ten years of GOME/ERS-2 total ozone data-The new GOME data processor (GDP) version 4: 1. Algorithm description, J. Geophys. Res., 111, D07307, doi:10.1029/2005JD006375, 2006. 7002

Vrekoussis, M., Wittrock, F., Richter, A., and Burrows, J. P.: GOME-2 observations of oxygenated VOCs: what can we learn from the ratio glyoxal to formaldehyde on a global scale?, Atmos. Chem. Phys., 10, 10145–10160, doi:10.5194/acp-10-10145-2010, 2010. 7021

Wagner, T., Beirle, S., Grzegorski, M., and Platt, U.: Global trends (1996-2003) of total column precipitable water observed by Global Ozone Monitoring Experiment (GOME) on ERS-2 and their relation to near-surface temperature, J. Geophys. Res., 111, D12102, doi:10.1029/2005JD006523, 2006. 7012

AMTD
8, 6993–7056, 2015

Wang, P., Stammes, P., van der A, R., Pinardi, G., and van Roozendael, M.: FRESCO+: an improved O_2 A-band cloud retrieval algorithm for tropospheric trace gas retrievals, Atmos. Chem. Phys., 8, 6565–6576, doi:10.5194/acp-8-6565-2008, 2008. 7014

Wang, P., Tuinder, O. N. E., Tilstra, L. G., de Graaf, M., and Stammes, P.: Interpretation of FRESCO cloud retrievals in case of absorbing aerosol events, Atmos. Chem. Phys., 12, 9057–9077, doi:10.5194/acp-12-9057-2012, 2012. 7016

Wentz, F. J. and Meissner, T.: AMSR-E Ocean Algorithms; Supplement 1, Report 051707, Remote Sensing Systems, Santa Rosa, CA, 2007. 7013

Wittrock, F., Richter, A., Oetjen, H., Burrows, J. P., Kanakidou, M., Myriokefalitakis, S., Volkamer, R., Beirle, S., Platt, U., and Wagner, T.: Simultaneous global observations of glyoxal and formaldehyde from space, Geophys. Res. Lett., 33, L16804, doi:10.1029/2006GL026310, 2006. 7021

World Meteorological Organization 2011: Scientific Assessment of Ozone Depletion: 2010, Global Ozone Research and Monitoring Project-Report, 52, WMO, Geneva, Switzerland, 516 pp., 2011. 7004

World Meteorological Organization 2014: Assessment for Decision-Makers: Scientific Assessment of Ozone Depletion: 2014, Global Ozone Research and Monitoring Project – Report No. 56, Geneva, Switzerland, 2014. 6999

AMTD
8, 6993–7056, 2015

Table 1. O3M SAF GOME-2 L2 products available to users, a summary table. Inst column refers to the instrument: A is GOME-2A, B is GOME-2B and A & B product is available both for GOME-2A and for GOME-2B instruments.

Product	Unit	Target accuracy	Spatial resolution[1]	Type	Dissemin.[2]	Inst[3]
Total ozone	DU	4/6 %[4]	80 km × 40 km	Column	NRT, OI	A & B
High res. ozone	DU	20 %	80 km × 40 km	Profile[5]	NRT, OI	A & B
Low res. ozone	DU	15/30 %[6]	640 km × 40 km[7]	Profile[5]	NRT, OI	A & B
Total NO_2	molec cm^{-2}	3–5 × 10^{14}	80 km × 40 km	Column	NRT, OI	A & B
Trop. NO_2	molec cm^{-2}	20 %	80 km × 40 km	Column	NRT, OI	A & B
Total SO_2	molec cm^{-2}	50 %[8]	80 km × 40 km	Column	NRT, OI	A & B
Total BrO	molec cm^{-2}	30 %	80 km × 40 km	Column	OI	A & B
Total HCHO	molec cm^{-2}	50 %	80 km × 40 km	Column	OI	A & B
Total H_2O	kg m^{-2}	10 %	80 km × 40 km	Column	OI	A & B
Absorbing Aerosol Index	unitless	0.5	80 km × 40 km	Index	NRT, OI	A & B
AAI from PMD	unitless	0.5	10 km × 40 km	Index	NRT, OI	A & B
Off-line UV Index	unitless	20 %	0.5° × 0.5°	Index	OI	B
Off-line UV daily dose[9]	kJ m^{-2}	20 %	0.5° × 0.5°	Surface	OI	B
Off-line UV max. dose[9]	mW m^{-2}	20 %	0.5° × 0.5°	Surface	OI	B
Off-line NO_2 photolysis	1 s^{-1}	20 %	0.5° × 0.5°	Surface	OI	B
Off-line O_3 photolysis	1 s^{-1}	20 %	0.5° × 0.5°	Surface	OI	B
NRT UVI clear	W m^{-2}	10 %	0.25° × 0.25°	Index	NRT	B
NRT UVI cloud	W m^{-2}	10 %	0.25° × 0.25°	Index	NRT	B
LER, MSC and PMD[10]	unitless	0.04	0.5° × 0.5°	Index	DR	A

[1] Spatial resolution: Nominal MSC (Main Science Channels) pixel size for GOME-2B is 80 km × 40 km whereas for GOME-2A it's 40 km × 40 km. For PMD (Polarization Measurement Device) the corresponding resolutions are 10 km × 40 km and 5 km × 40 km. Only the GOME-2B resolution is indicated in this column.
[2] NRT (Near Real Time), OI (Off-line), DR (Data Record).
[3] Instrument: A refers to GOME-2A and B to GOME-2B.
[4] 4 % for SZA < 80° and 6 % for SZA > 80°.
[5] Ozone profiles up to 0.001 hPa, 40 layers.
[6] 15 % for stratosphere and 30 % for troposphere.
[7] 80 × 40 ground pixel resolution follows the integration time of the 1B channel whereas 640 × 40 integration time follows UV wavelengths.
[8] SZA < 70°.
[9] Offline UV product has the following weighting functions: Erythemal (CIE), plant response, DNA damage, UVA, UVB, D-vitamin.
[10] Lambertian Equivalent Reflectivity. Resolution for MSC (Main Science Channels) product is 1° × 1° and for PMD product 0.5° × 0.5°.

AMTD
8, 6993–7056, 2015

Table 2. GOME-2/Metop trace gas column and cloud products generated by the O3M-SAF, with the corresponding wavelength regions used for the retrieval. The cloud products are internal products used in the retrieval of the other products.

Product	Wawelength region
Ozone column	325.0–335.0 nm
NO_2 column	425.0–450.0 nm
BrO column	332.0–359.0 nm
SO_2 column	315.0–326.0 nm
H_2O column	614.0–683.2 nm
HCHO column	328.5–346.0 nm
Cloud fraction column	300–800 nm (PMD-p)
Cloud top height (pressure) and albedo (optical thickness)	758–771 nm

AMTD
8, 6993–7056, 2015

Table 3. WMO GTS bulletin headers.

	TTAAAii	CCCC	CF
Trace Gases	IUCX01	EDLR	FM 94-BUFR
Ozone profiles	TTAAii	EHDB	FM 94-BUFR

AMTD
8, 6993–7056, 2015

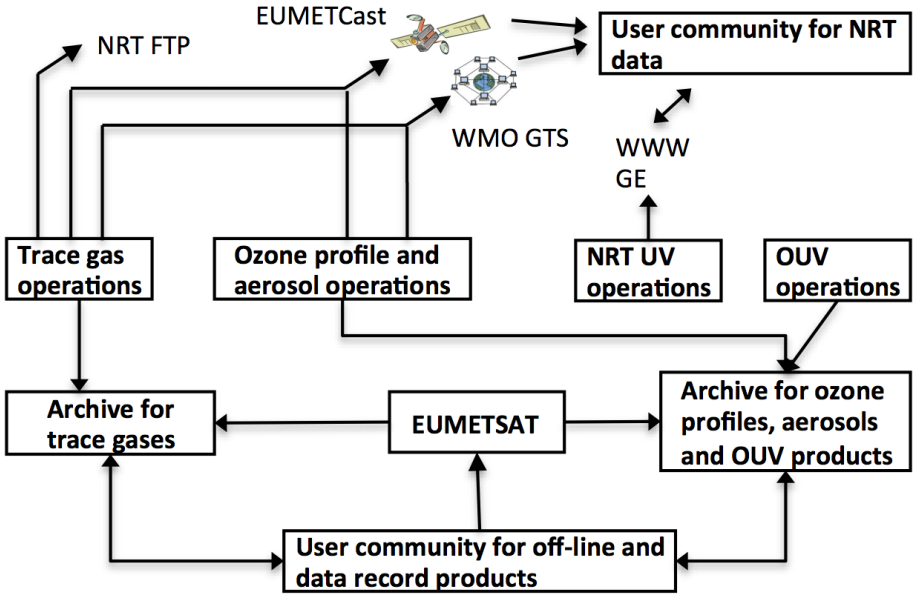

Figure 1. O3M SAF delivery scheme for the GOME-2 products. The off-line and data set users may place order in EUMETSAT Data Center interface or directly to archive centers. GE refers to Google Earth.

AMTD
8, 6993–7056, 2015

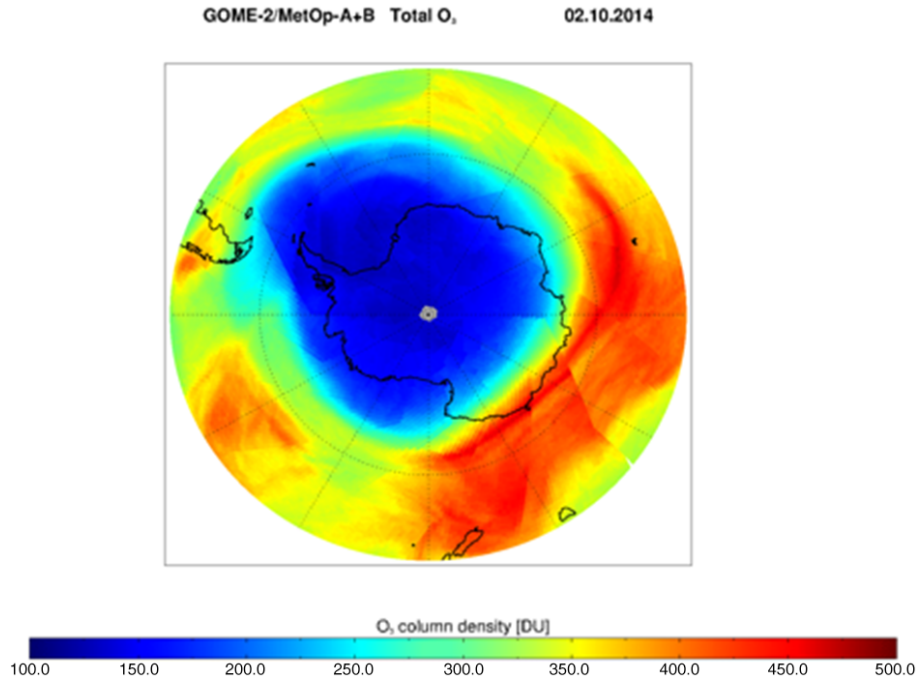

Figure 2. Total ozone map for 2 October 2014 based on data from GOME-2A and GOME-2B instruments.

AMTD
8, 6993–7056, 2015

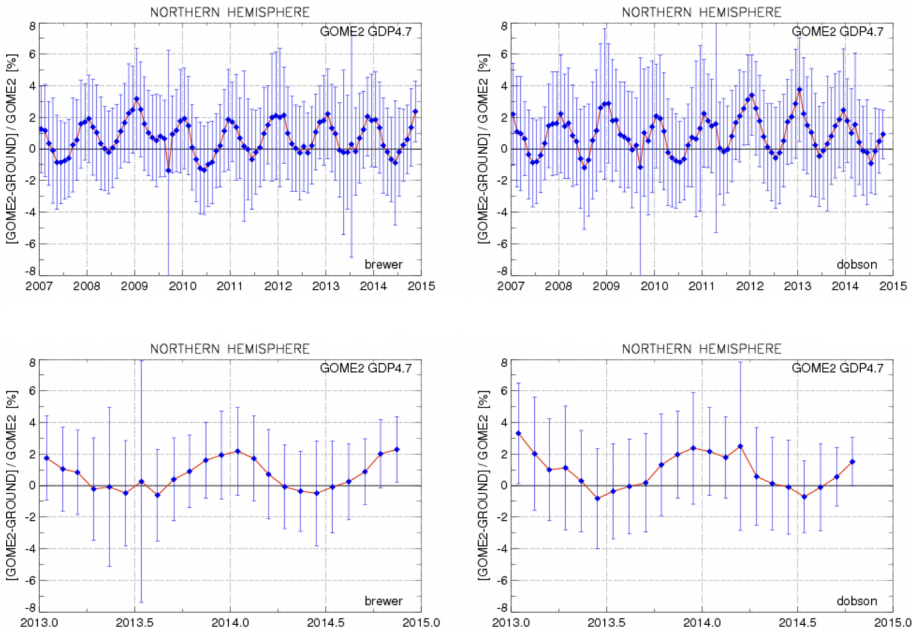

Figure 3. Monthly mean differences between GOME-2A (upper) and GOME-2B (lower) vs. ground-based total Ozone columns; Brewer comparisons in the left column and Dobson comparisons in the right.

AMTD
8, 6993–7056, 2015

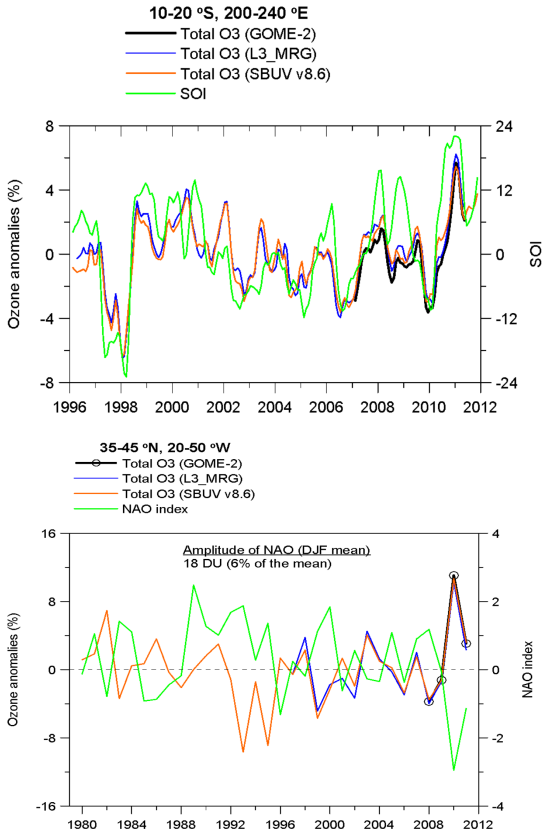

Figure 4. Time series of SOI (upper panel) and NAO (lower panel) and the related total ozone signals for the data sets indicated.

AMTD
8, 6993–7056, 2015

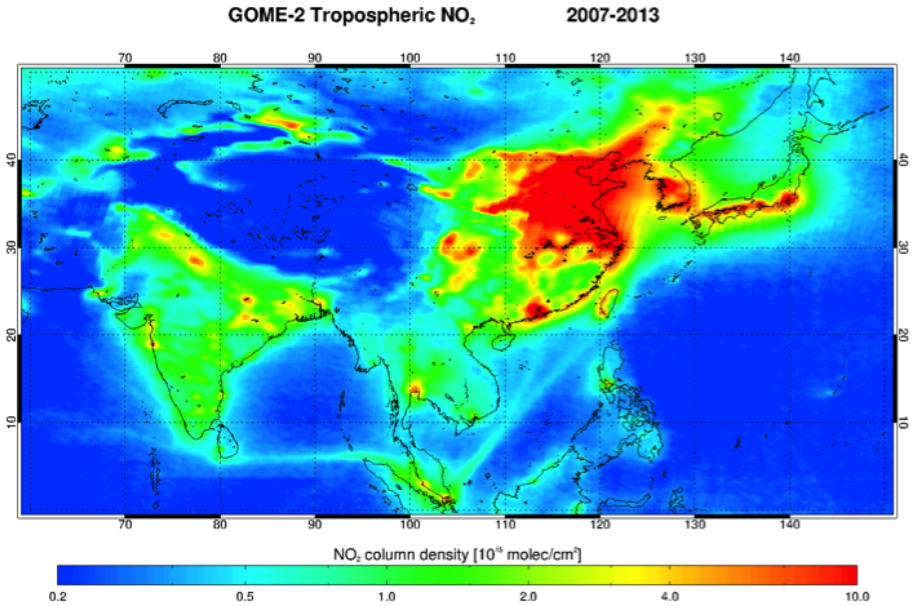

Figure 5. Average tropospheric NO_2 columns over East Asia measured by GOME-2 for 2007–2013.

AMTD
8, 6993–7056, 2015

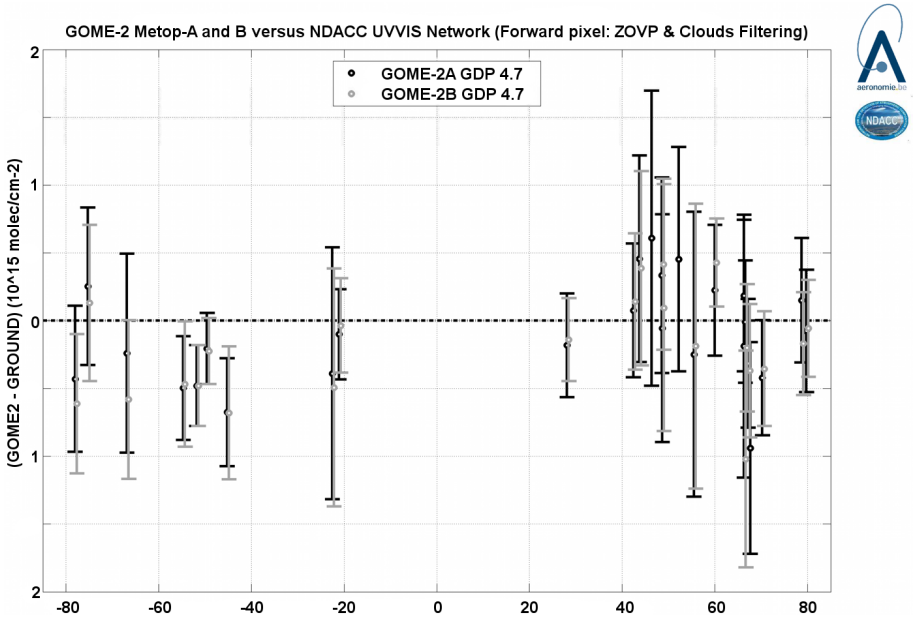

Figure 6. Example of total (stratospheric) NO_2 validation: pole-to-pole structure of the median absolute difference between NO_2 column data retrieved from GOME-2A/B (GDP 4.7) and from 25 ground-based zenith-sky DOAS spectrometers archiving consolidated data to NDACC DHF, calculated over 2007–2014 for GOME-2A and 2013–2014 for GOME-2B.

AMTD
8, 6993–7056, 2015

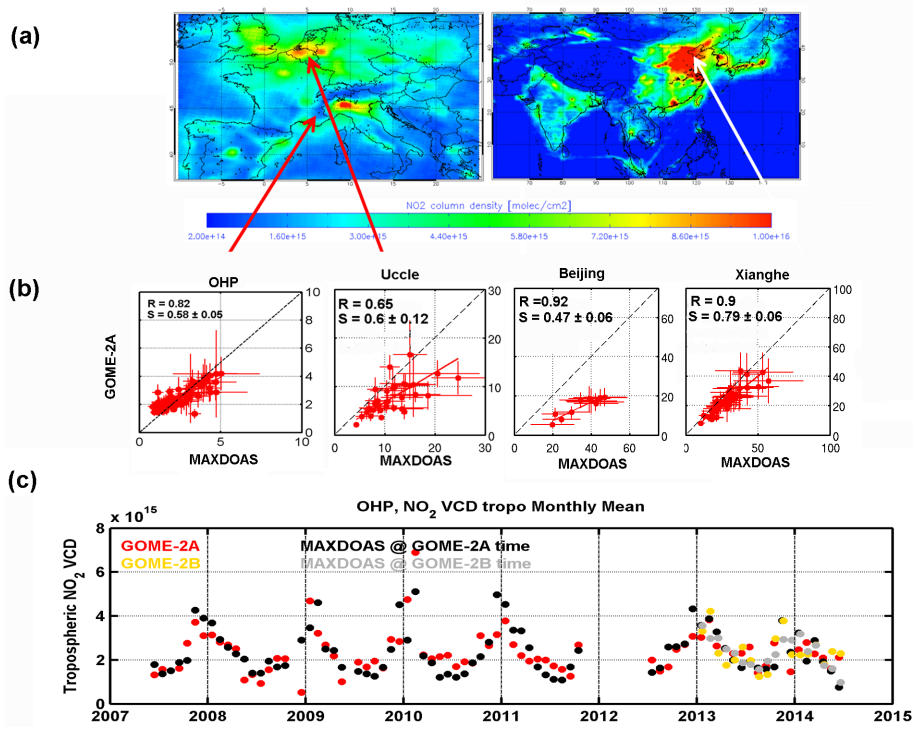

Figure 7. Example of tropospheric NO_2 validation: **(a)** maps of tropospheric NO_2 from GOME-2 and the location of 3 BIRA-IASB MAXDOAS stations: OHP, Uccle and Xianghe. **(b)** The correlation plots are given for each station for GOME-2A (OHP from June 2007 to February 2014, Uccle from May 2011 to May 2014, Beijing from June 2008 to April 2009, Xianghe from March 2010 to December 2013), while **(c)** a time-serie of MAXDOAS, GOME-2A and GOME-2B is given for OHP station.

AMTD
8, 6993–7056, 2015

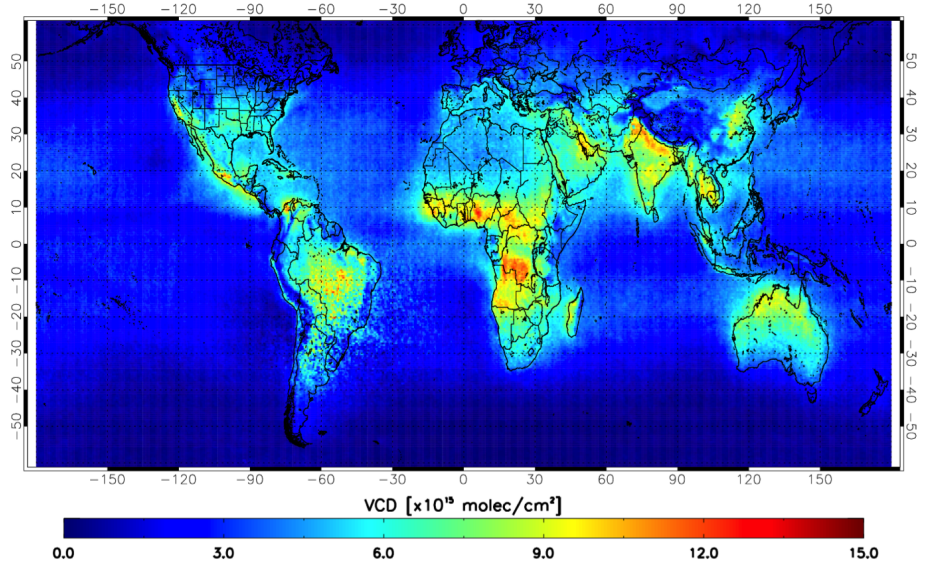

Figure 8. Averaged tropospheric H_2CO columns for 2013 as measured by GOME-2 on MetOp-B.

AMTD
8, 6993–7056, 2015

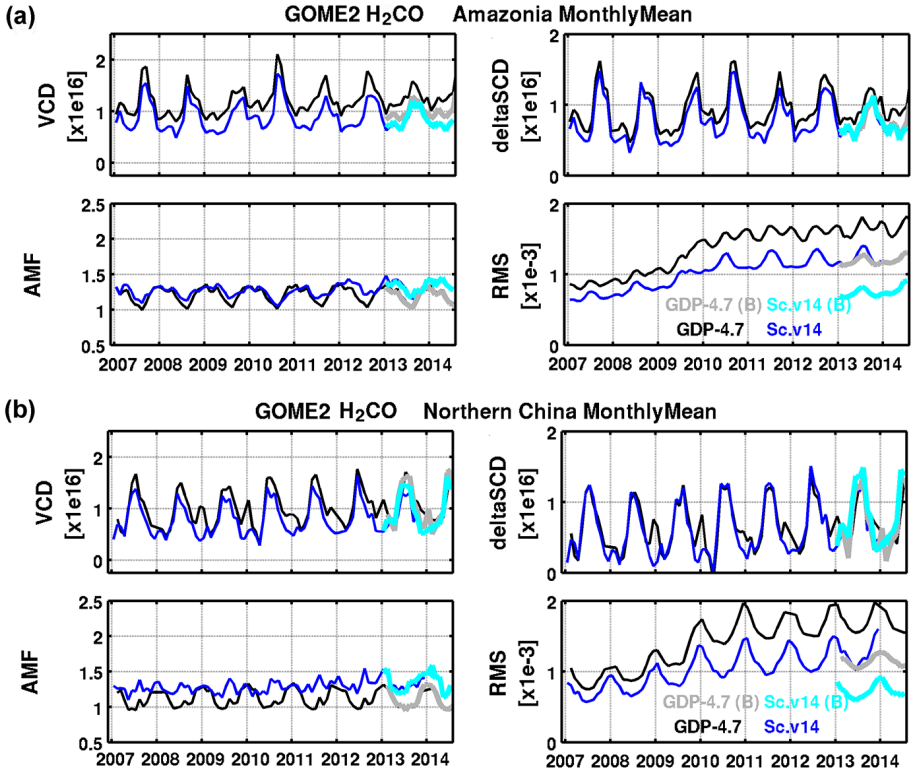

Figure 9. Example of H_2CO end-to-end validation for **(a)** the Guatemala and **(b)** Northern China regions. Monthly means comparisons of GOME-2A and GOME-2B GDP data (black and grey) are compared to the corresponding scientific algorithm v14 (blue and cyan) for every step of the VCD retrieval: the normalized slant columns (delta SCD), the DOAS fit RMS (indicator of the fit quality), the cloud-corrected (total tropospheric) air mass factor AMF and the tropospheric vertical column VCD.

AMTD
8, 6993–7056, 2015

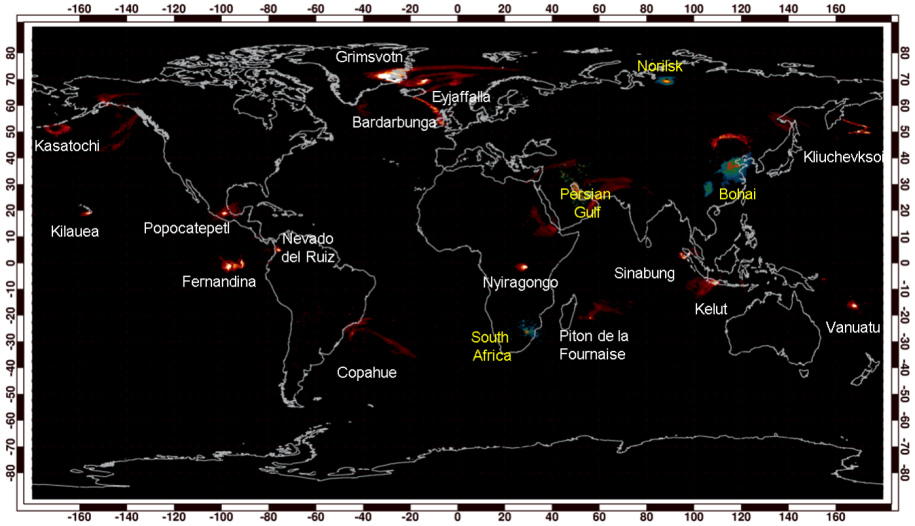

Figure 10. Major SO_2 emissions detected by the GOME-2 instruments since 2007. Volcanic eruption are marked in white, while anthropogenic SO_2 emissions are in yellow.

AMTD
8, 6993–7056, 2015

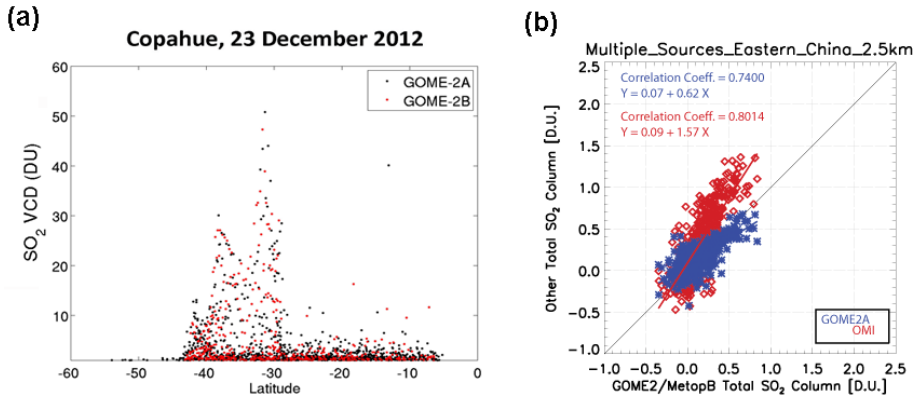

Figure 11. Example of SO_2 validation activities: **(a)** comparisons of SO_2 columns retrieved from GOME-2A and GOME-2B for the Copahue eruption, as a function of latitude and **(b)** scatter plot of anthropogenic SO_2 (assuming a 2.5 km plume height) over Eastern China from GOME-2B (*x* axis) and respectively GOME-2A (blue) and OMI (red).

AMTD
8, 6993–7056, 2015

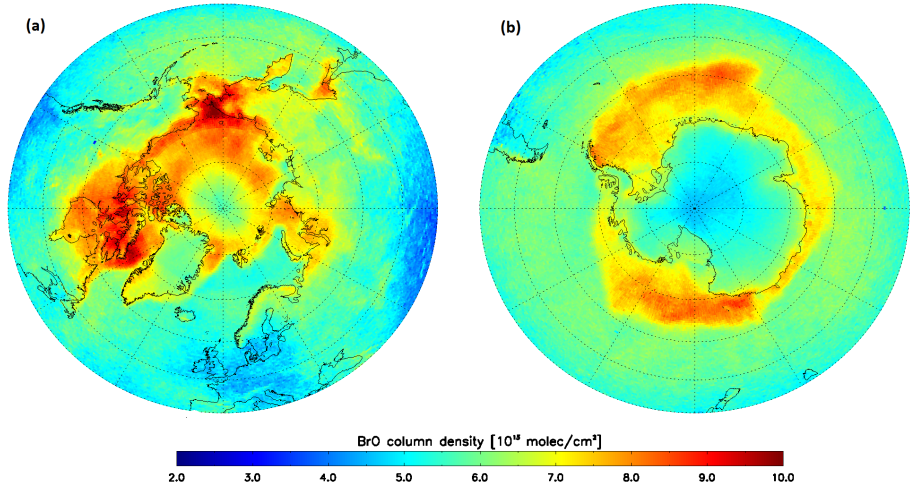

Figure 12. Monthly averaged total BrO columns **(a)** over the Arctic, April 2007 and **(b)** Antarctic, October 2007.

AMTD
8, 6993–7056, 2015

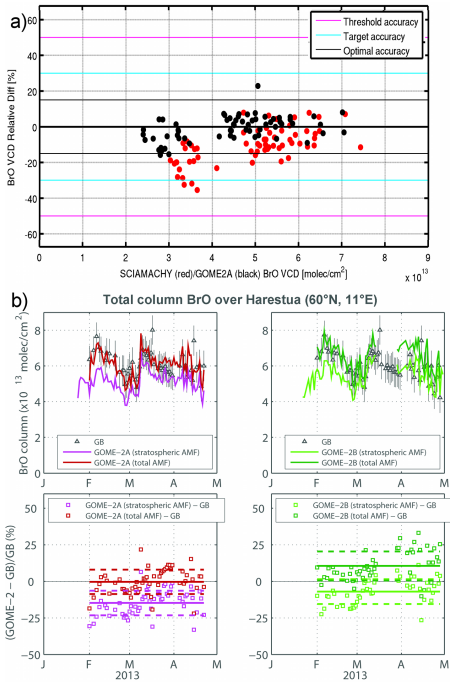

Figure 13. Example of BrO validation: **(a)** monthly averaged BrO VCD relative difference between GOME-2B (red) and GOME-2A (black) against SCIAMACHY as a function of SCIAMACHY/GOME-2A BrO VCD, for 14 sites from pole-to-pole over the period December 2012–April 2013. **(b)** Comparison of GOME-2 (A and B) and ground-based total BrO columns at Harestua (60° N, 11° E) in February–April 2013. The satellite results labeled "total AMF" are calculated using the stratospheric and tropospheric AMFs weighted by the BrO column contribution in both layers as retrieved from the ground-based measurements. The relative differences (squares) and mean biases (solid lines) appear in the lower plots. The number of coincidences is 55 for GOME-2A and 49 for GOME-2B.

AMTD
8, 6993–7056, 2015

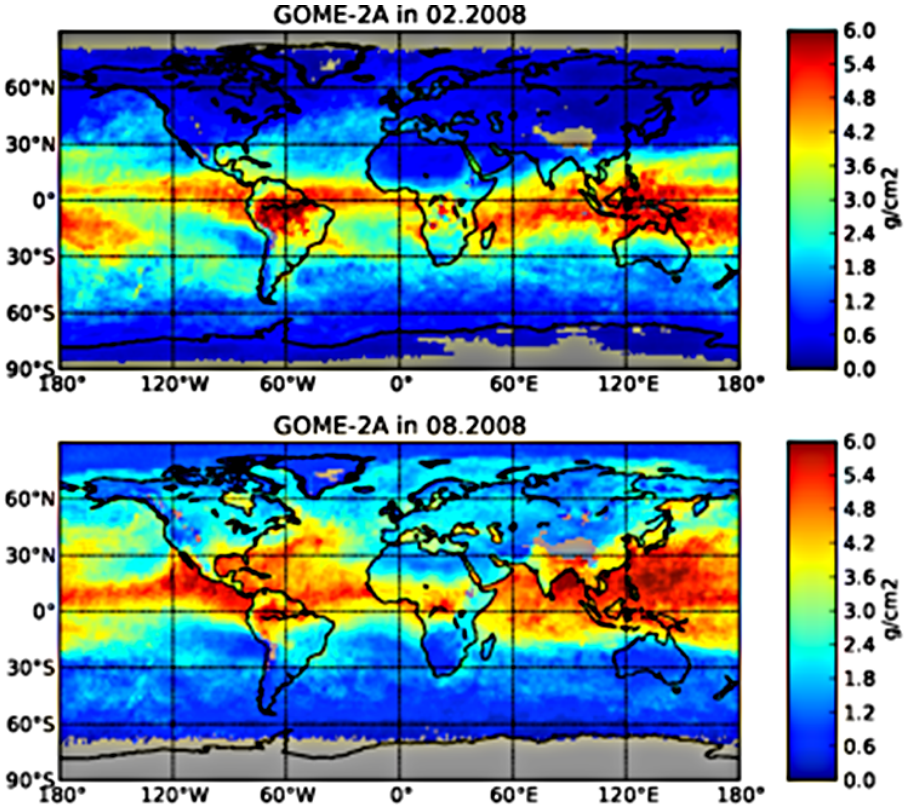

Figure 14. Monthly mean maps of total column water vapour from GOME-2A for February 2008 (on the top) and August 2008 (on the bottom). Only cloud-screened data have been used.

AMTD
8, 6993–7056, 2015

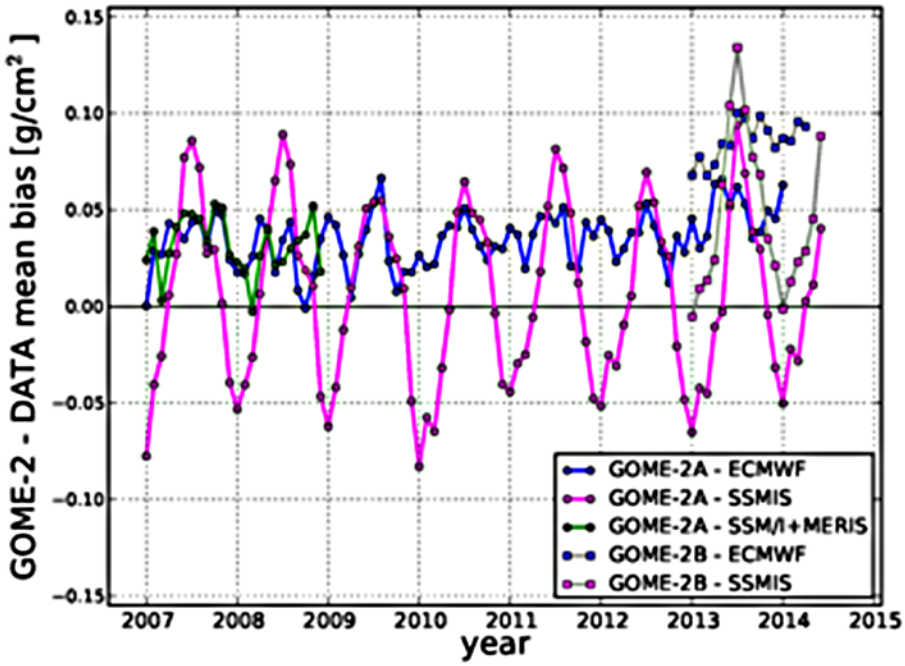

Figure 15. Global monthly mean bias between GOME-2/MetOp-A and 3 independent TCWV data sets for the period January 2007–June 2014, depending on availability of the reference data. The comparison is performed against ECMWF ERA-Interim reanalysis (blue points), SSMIS F16 satellite (magenta points, only over ocean) and combined SSM/I + MERIS data set (green points). Colored squares and gray lines show the bias between the most recent GOME-2/MetOp-B observations and the ECMWF and SSMIS data sets.

AMTD
8, 6993–7056, 2015

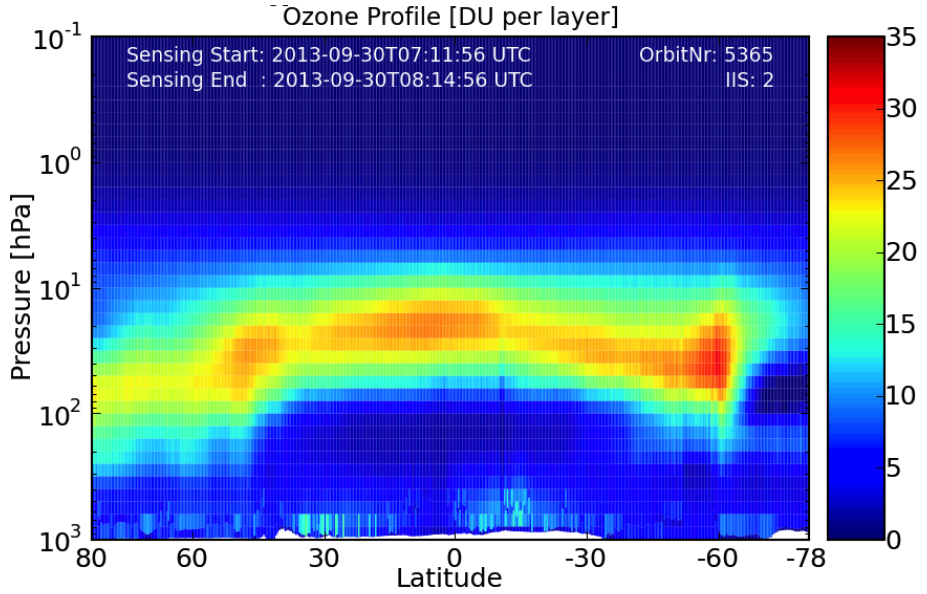

Figure 16. Vertical ozone profiles from GOME-2 on Metop-B, as a vertical cross section along an orbit from north to south. The measurements end in a location over the Antarctica where the Southern Hemisphere spring ozone hole is present, indicated by low ozone values in the stratosphere.

AMTD
8, 6993–7056, 2015

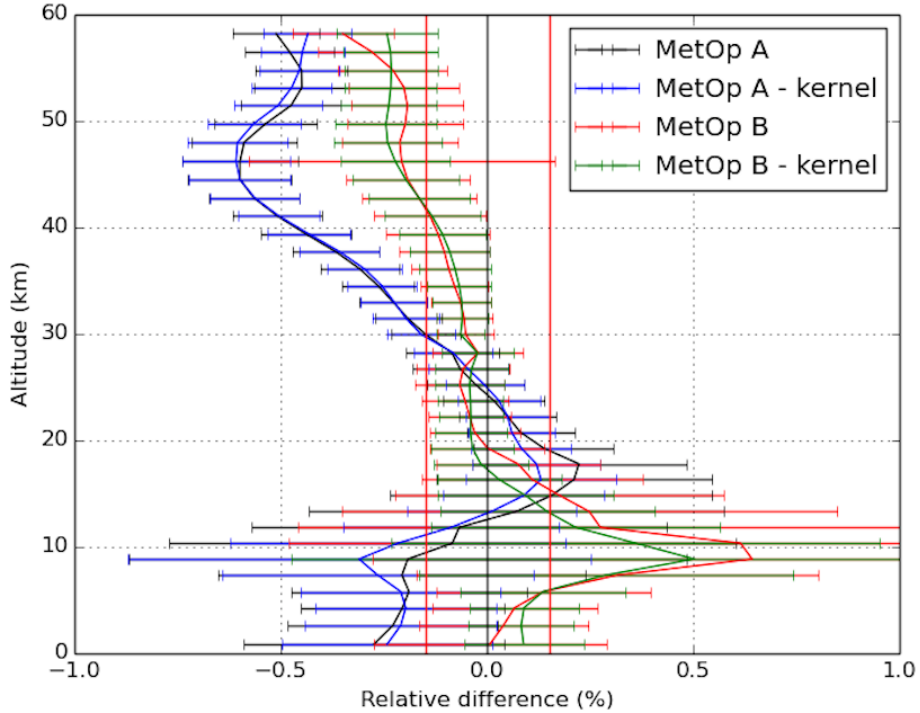

Figure 17. Relative differences between GOME-2A and GOME-2B ozone profiles (CR) and corresponding ground based measurements. Shown is an average over all data from the years 2013 and 2014 for northern midlatitude stations. Up to 30 km altitude, all available ozone sondes are used for comparison, and above it is an average of two lidar (Hohenpeissenberg and Haute Provence) and two microwave stations (Bern and Payerne). The black (GOME-2A) and red (GOME-2B) curves are raw data, while the blue (GOME-2A) and green (GOME-2B) curves show data smoothed with the GOME-2 averaging kernel and a-priori information.

AMTD
8, 6993–7056, 2015

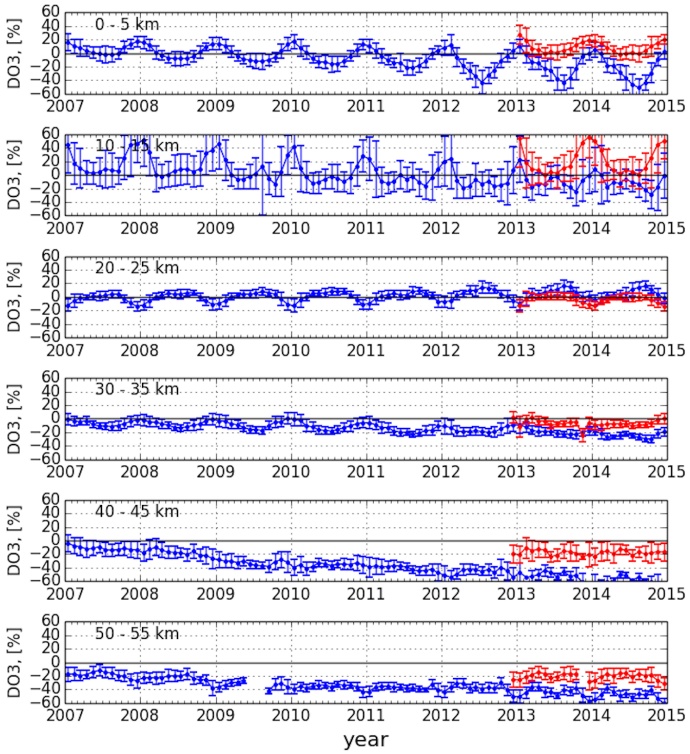

Figure 18. Time series of the relative differences between GOME-2A ozone profiles (CR) and corresponding ground based measurements. Shown are monthly mean values and their standard deviations. The data are averaged over all available stations at northern midlatitudes. At the three lower altitude layers, ozone sondes are used for comparison, and at the higher levels, two lidar (Hohenpeissenberg and Haute Provence) and two microwave stations (Bern and Payerne). The blue curves are for GOME-2A and the red ones for GOME-2B. All data are smoothed, by applying the GOME-2 averaging kernel and a-priori information.

AMTD
8, 6993–7056, 2015

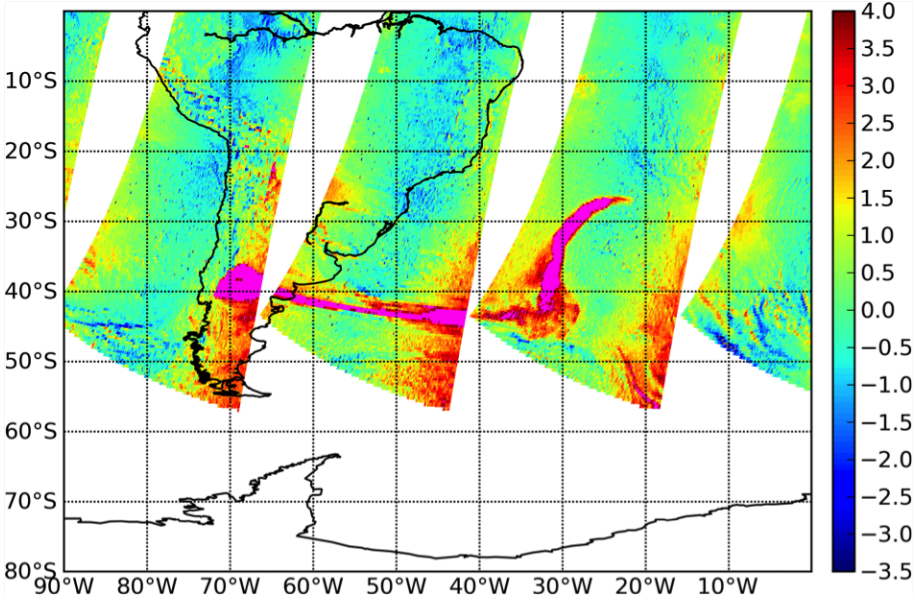

Figure 19. Absorbing Aerosol Index from the PMD bands from Metop-A on 6 June 2011 over the south Atlantic Ocean. The plume of aerosol originates from an eruption of the Puyehue volcano.

AMTD
8, 6993–7056, 2015

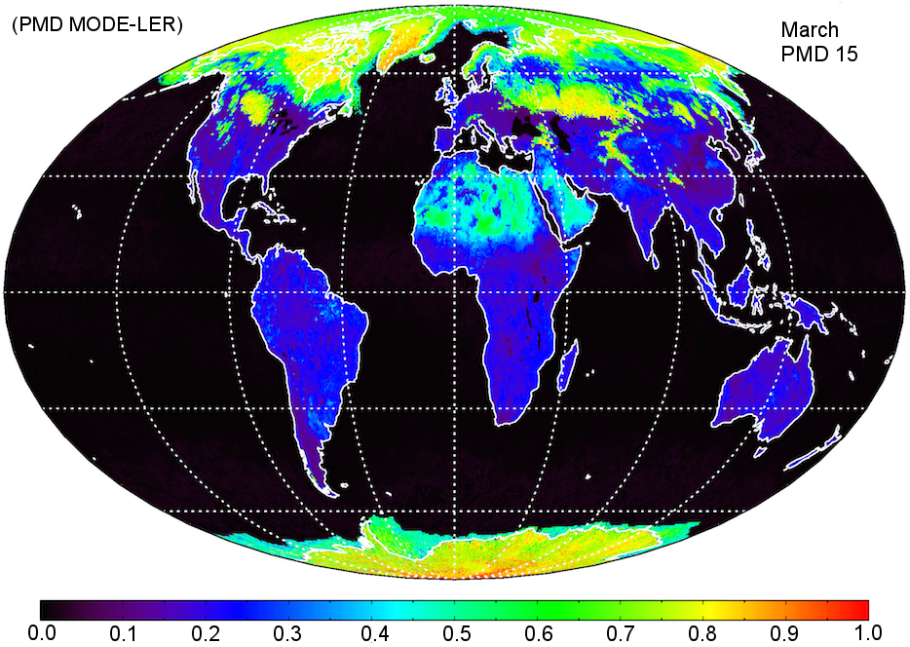

Figure 20. Example of the GOME-2 surface LER determined from PMD band 15 (centred around 799 nm) for March. The snow cover on northern latitudes as well as Sahara desert are clearly seen.

AMTD
8, 6993–7056, 2015

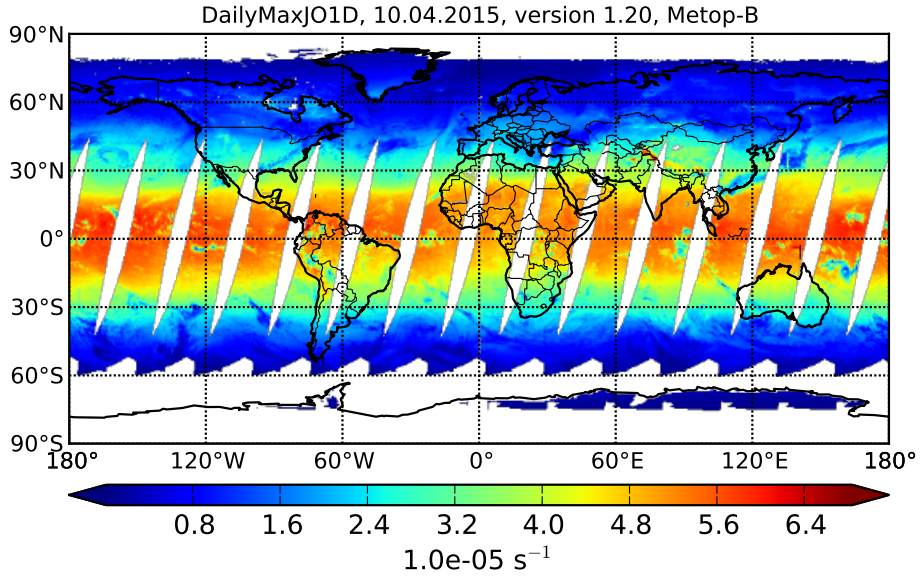

Figure 21. Daily maximum photolysis frequency of ozone j_{O^1D} at the ground level obtained from Metop-B and NOAA-19 data on 10 April 2015. Global coverage of the product is limited by the swath of the GOME-2 instrument leaving stripes at low latitudes. The polar night and the maximum solar zenith angle for cloud processing limit the coverage at high latitudes while cloud-free values are accepted for the Antarctic and Greenland ice sheets.

AMTD
8, 6993–7056, 2015

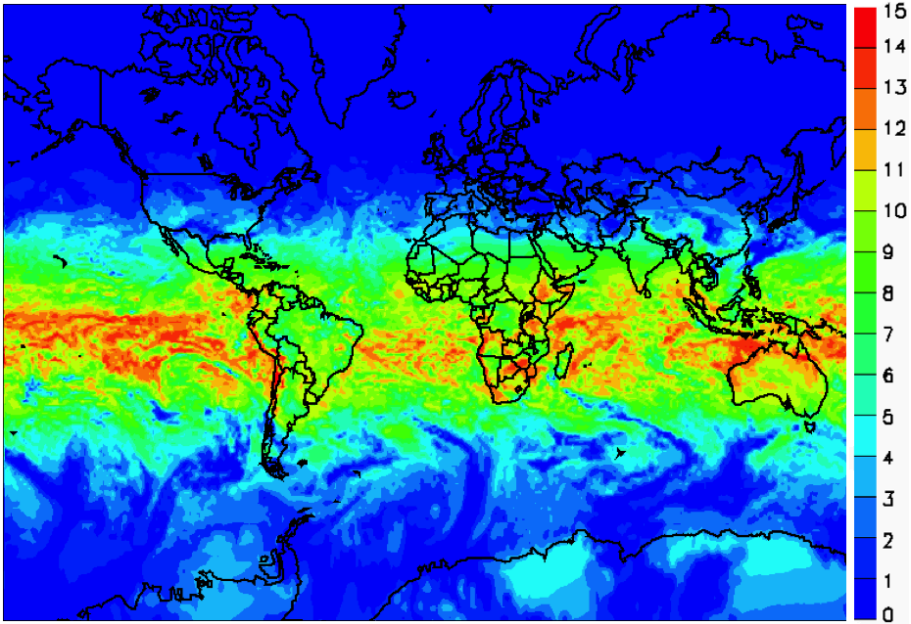

Figure 22. Global map of the NRT Cloud corrected UV Index on 2 November 2013.

AMTD
8, 6993–7056, 2015